

SHEAR ZONE RELATED TALC MINERALIZATIONS IN THE VEITSCH NAPPE OF THE EASTERN GREYWACKE ZONE (EASTERN ALPS, AUSTRIA)

Anke WÖFLER^{1*)}, Walter PROCHASKA¹⁾ & Harald FRITZ²⁾

DOI: 10.17738/ajes.2015.0004

KEYWORDSGreywackezone
talc formation
Eastern Alps
shearzone¹⁾ University of Leoben, Peter-Tunner-Str. 5, 8700 Leoben, Austria;²⁾ University of Graz, Heinrichstr. 26, 8010 Graz, Austria;^{*)} Corresponding author, anke.woelfler@unileoben.ac.at**ABSTRACT**

Shear zones are zones of enhanced fluid flow and may act as pathways for mineralizing fluids. The occurrence of talc may be related to such shear zones. Magnesite and talc deposits in the Eastern Greywacke zone were investigated to understand the role of faults to the occurrence of talc. The deposits Veitsch, Wald am Schober and Lassing are of Mg carbonate hostrocks and vary in their talc content. Geochemical analysis, stable isotopes and fluid inclusion studies were performed to yield indications on kind, origin and temperature of the talc mineralizing fluid. The results have shown that the precipitation of talc in the Eastern Greywacke zone is related to increasing deformation and temperature along shear zones. The magnesite deposit of Veitsch is characterized by brittle low temperature deformation features and analyses have demonstrated that fluid temperatures are commonly low (~180°C) similar to samples of host rocks outside the deposits. The magnesite deposit of Wald am Schober contains minor occurrences of talc along discrete shear zones. The deposit is characterized by ductile deformation features. Temperatures of the mineralizing fluids are significantly higher (~250°C). At the former Lassing talc mine talc occurs within large shear zones and yield features of high deformation. All three deposits are in vicinity to fault zones (Mur-Mürz-Fault, Paltental-Liesingtal-Fault, SEMP) that were active during Miocene escape tectonics. In the case of Wald am Schober extensional tectonics following Eo-alpine (Cretaceous) orogeny may have played an important role. The fluids that lead to the precipitation of talc are of metamorphic origin. It can be concluded that major fault zones as well as nappe boundaries have a great impact as fluid pathways and zones of deformation where mineralizations are largely enriched.

Scherzonen sind Zonen, die typisch sind für einen erhöhten Fluidfluss und als Wege für mineralisierende Fluide dienen. Talkvorkommen können an solche Scherzonen gebunden sein. Magnesit- und Talkvorkommen in der östlichen Grauwackenzone wurden untersucht, um die Rolle der Störungen für die Talkbildung zu verstehen. Die Lagerstätten Veitsch, Wald am Schober und Lassing bestehen aus Mg-Karbonat-Gesteinen, variieren aber jeweils in ihrem Talkgehalt. Geochemieanalysen sowie Studien zu Stablen Isotopen und Flüssigkeitseinschlüssen wurden vorgenommen, um Hinweise auf Art, Herkunft und Temperatur der talkausfällenden Fluide zu erhalten. Die Studie hat gezeigt, dass die Ausfällung von Talk in der östlichen Grauwackenzone im Zusammenhang mit erhöhter Deformation und Temperatur entlang von Störungen steht. Die Magnesitlagerstätte Veitsch zeichnet sich durch spröde Niedrigtemperatur-Deformations-Charakteristika aus und Analysen haben gezeigt, dass die Fluidtemperaturen ähnlich niedrig (~180°C) sind, wie bei den die Lagerstätten umgebenden Gesteinen. Die Magnesitlagerstätte Wald am Schober zeigt geringe Talkvorkommen entlang von diskreten Scherzonen auf. Die Lagerstätte ist von duktilen Deformationsmerkmalen gekennzeichnet. Die Analysen an Proben der Lagerstätte haben ergeben, dass die Temperaturen des mineralisierenden Fluids wesentlich höher (~250°C) sind. In der ehemaligen Talklagerstätte Lassing kommt der Talk in großen Scherzonen vor, welche Hinweise auf hohe Deformation geben. Alle drei Lagerstätten sind in Zusammenhang mit Störungen (Mur-Mürz-Furche, Paltental-Liesingtal-Störung, SEMP), die während der miozänen lateralen Extrusionstektonik aktiviert wurden, zu sehen. Im Falle von Wald am Schober kann auch die Dehnungstektonik im Zuge der Eoalpinen Gebirgsbildung eine wichtige Rolle spielen. Die Fluide, die zur Talkbildung geführt haben, sind metamorphogener Herkunft. Es kann geschlussfolgert werden, dass große Störungen einen wesentlichen Einfluss haben in Form von Fluidwegen und Deformationszonen.

1. INTRODUCTION

Talc belongs to the commercially most important minerals worldwide, however its petrogenesis, occurrence and timing of formation are poorly understood. Talc occurs most abundantly in metamorphosed ultramafic rocks and the environments of talc formation have been described in detail by Evans and Guggenheim (1991; and references therein). Further Mg-carbonates such as siliceous dolomitic limestone and magnesite serve as hostrocks. In such rock suites talc may form under

prograde as well as retrograde metamorphic conditions. These carbonate hostrocks may be subject to hydrothermal alteration (Moine et al., 1989) with Si-rich fluids reacting with the Mg-carbonates: $3\text{CaMg}(\text{CO}_3)_2 + 4\text{SiO}_2 + \text{H}_2\text{O} \rightarrow \text{Mg}_3\text{Si}_4\text{O}_{10}(\text{OH})_2 + 3\text{CaCO}_3 + 3\text{CO}_2$ (in the case of dolomite hostrocks) and $3\text{MgCO}_3 + 4\text{SiO}_2 + 2\text{H}_2\text{O} \rightarrow \text{Mg}_3\text{Si}_4\text{O}_{10}(\text{OH})_2 + 3\text{CO}_2$ (in the case of magnesite hostrocks). In addition zones of intense deformation, where fluid flow is elevated, are prone to the for-

mation of talc. Examples for such talc deposits are Trimouns in the French Pyrenees (Moine et al., 1989 and Boulvais, 2006) and Rabenwald and Lassing in the Eastern Alps (Prochaska, 1989, 2000; Neubauer, 2001). To a smaller extent talc forms in hydrothermal and surface environments and in high pressure rocks.

In this study we investigate three talc deposits in the Eastern Alps to develop a model for the conditions, the mechanisms and timing of talc formation. Additionally we will discuss the relationship of talc mineralization with the regional tectonic regime. For this purpose we performed geochemical analysis of major, minor and trace elements, stable isotope studies on carbonates and quartz as well as fluid inclusion measurements.

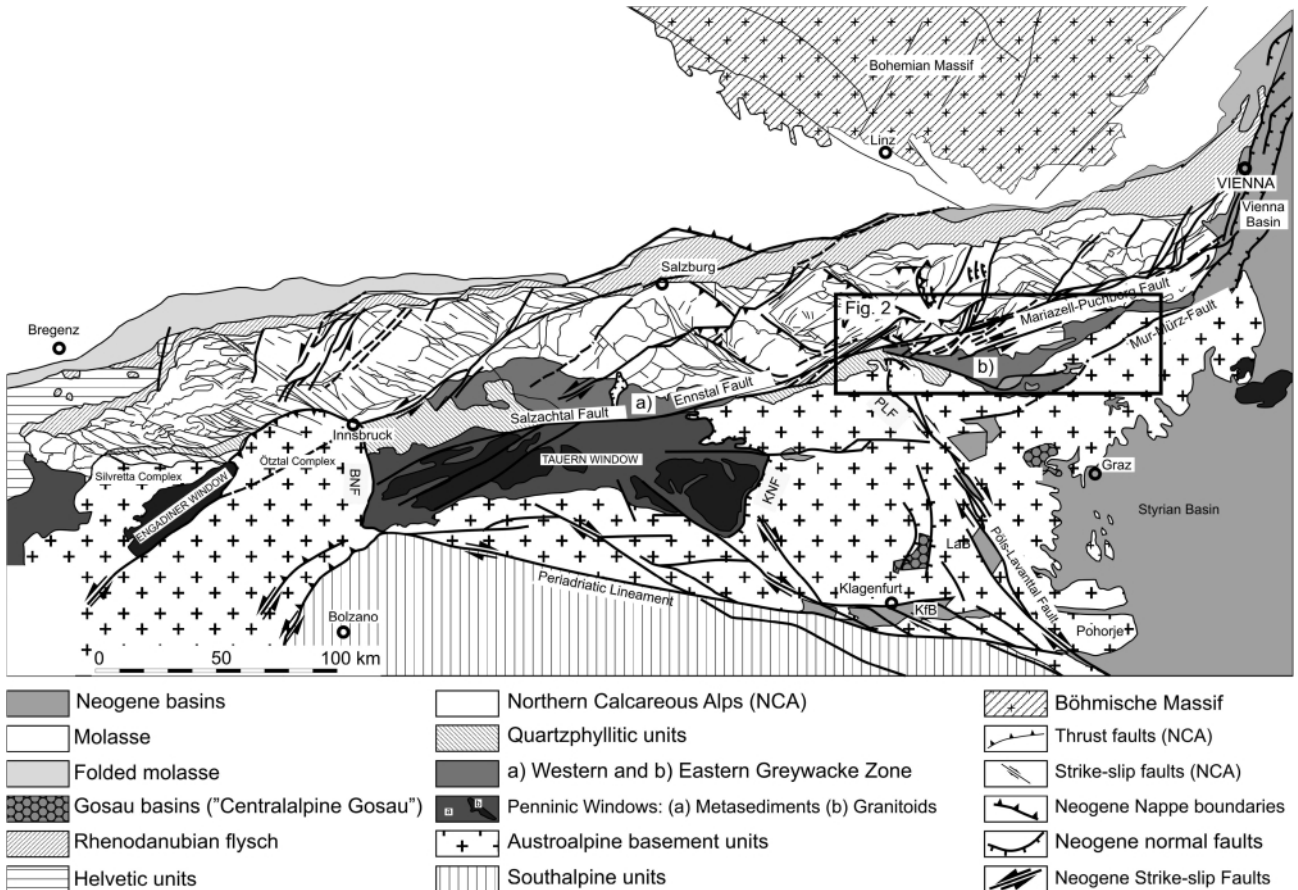
2. METHODS

Whole rock geochemical analysis of major, minor and trace elements were performed at Act Labs, Canada. Prior samples were prepared at the University of Leoben by crushing and grinding. Analytical procedures are described by Act Labs as follows: Samples are analyzed in a batch system, wherein each batch contains a reagent blank, certified reference material and 17% replicates. Samples are then mixed with a flux of lithium metaborate and lithium tetraborate and fused in an induction furnace. The molten melt is immediately poured into a solution of 5% nitric acid containing an internal standard and

mixed continuously until completely dissolved. The samples are run for major oxides and selected trace elements (including REE) on a combination simultaneous/sequential Thermo Jarrel-Ash ENVIRO II ICP or a Varian Vista 735 ICP. Calibration is performed using 7 prepared USGS and CANMET certified reference materials. One of the 7 standards is used during the analysis for every group of ten samples. Totals must be between 98.5% and 101%.

Analyses of carbon and oxygen isotope ratios of carbonates were performed at the stable Isotope laboratory at the University of Leoben. Samples were prepared by using a dentist drill. 0.2 – 0.3 mg of rockpowder was drilled and transferred into autosampler vials (Labco Exetainer vials) and sealed with butyl-rubber septa. The analyses were performed on a Thermo Fisher Delta V mass spectrometer employing a Finnigan Gas Bench II according to Spötl and Vennemann (2003). The samples were dissolved with anhydrous H3PO4 (density 1.91 g/cm³) in a pressurised helium atmosphere at 70°C for 8 hours. Multiple measurements of in-house calcite reference material were used and precision of δ18O and δ13C measurement were yielded with ±0.07‰ and ±0.05‰ (1s, n=180), respectively. Oxygen isotope data are reported relative to Vienna Mean Ocean Water (VSMOW) and carbon isotopes relative to Vienna Pee Dee Belemnite (VPDB).

Analyses of oxygen isotope ratios of quartz were performed



KfB - Klagenfurt Basin, LaB - Lavantal Basin, BNF - Brenner Normal Fault, KNF - Katschberg Normal Fault, PLF - Paltental-Liesingtal-Fault
FIGURE 1: Geological sketch of the Eastern Alps. Modified after Linzer et al. (2002).

at the stable isotope laboratory at the University of Lausanne. Quartz samples were prepared by crushing and handpicking to yield grains free of impurities. Each aliquot (1-2 mg) was washed with distilled water and dilute HCl (10%) to remove calcite residuals. Oxygen was then extracted using a CO₂ laser-line and fluorine reagent (method according to Kase-mann et al., 2001). Isotopic composition of extracted oxygen was measured using a ThermoFinnigan MAT 253 mass spectrometer. Results were normalized against an in-house quartz standard (LS-1, 20-50 mesh, δ¹⁸O = 18.1‰ calibrated against NBS-28 of δ¹⁸O = 9.64‰). The standard reproduced to within an error of ±0,1‰. Oxygen isotope data are reported relative to Vienna Mean Ocean Water (VSMOW).

Crush leach analysis on fluid inclusions in quartz and carbonates was performed using ion-chromatography. The samples were crushed, thoroughly washed and handpicked. In addition quartz samples were treated with HNO₃ in a sand bath to remove possible contaminations. Sample size was 1.00 g given the dependency of the ion concentration from the number of fluid inclusion in one sample. The leaching process was performed with minor modifications according to Bottrell et al. (1988) and Prochaska (1997): Samples were grounded with 5 ml double distilled water in an agate mortar, filtered and transferred into suitable vials. Halogens and anions (F⁻, Br⁻, Cl⁻, I⁻, SO₄²⁻) were measured using a DIONEX DX- 500 system at Leoben University. Cations (Li⁺, Na⁺, K⁺, Mg²⁺, Ca²⁺) were analysed in the aliquots of the same solution.

3. GEOLOGY

Geologically, the Eastern Alps are the result of the still ongoing convergence between Europe and the Adriatic plate (e.g.

Collombet et al., 2002). The Eastern Alps consist of two major domains – (i) the Austroalpine nappes as part of the Adriatic plate and (ii) the Penninic units, that have been overthrust by the Austroalpine nappe stack throughout Eocene and Oligocene times (e.g. Neubauer et al., 2000). The Austroalpine consists of a pre-Carboniferous basement - in fact protolith ages date back until the Proterozoic (Schulz et al., 2004) or even the Archean (Neubauer et al., 2002) - and a Permomesozoic cover, such as the Northern Calcareous Alps (NCA) (Fig. 1). These units were affected by Variscan, Permian and later by Cretaceous metamorphism during the Eoalpine orogeny (e.g. Schuster and Stüwe, 2008, Thöni, 2006). During the Oligocene and Miocene, the footwall Penninic units such as the Tauern Window (Fig. 1), were tectonically exhumed from below the Austroalpine hanging wall (e.g. Frisch et al. 1998). This process, termed to as lateral extrusion (Ratschbacher et al. 1991a, b), was not only accompanied by the exhumation of the footwall, but also by enhanced fault activity and the formation of intramontane basins (Fig. 1, e.g. Sachsenhofer et al. 1997, 1998, 2000; Wölfler et al. 2011, 2012). Fault zones that accommodate the lateral escape are the Brenner- and Katschberg normal faults to the west and east of the Tauern Window, respectively (Selverstone, 1988; Genser and Neubauer, 1989; Scharf et al., 2013), as well as eastwest and north-south striking strike slip fault zones (Fig.1). The northern boundary of the extruding wedge is represented by the Salzach-Ennstal-Mariazell-Puchberg fault system (SEMP) (Fig. 1). Kinematic analysis revealed sinistral slip (Decker and Pesson, 1996; Linzer et al., 1997; Wang and Neubauer, 1996) accommodating a displacement of 60 km during Oligocene and Miocene times (Linzer et al., 1997, 2002). However, a re-

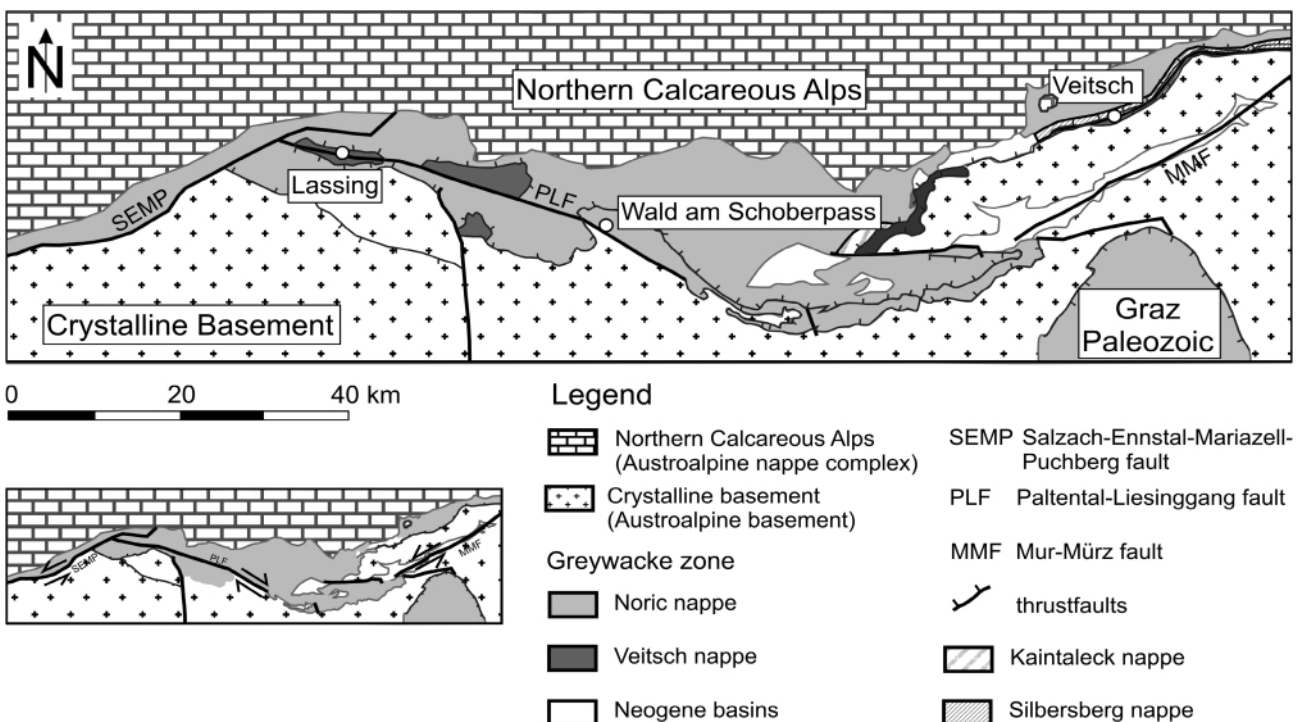


FIGURE 2: Geological sketch of the Eastern Greywacke zone. Modified after Rantitsch et al. (2004).

cent study by Plan et al. (2010) demonstrated that the SEMP is still active. The Periadriatic fault system (PAL) separates the Eastern- from the Southern Alps (Fig. 1). While to the south of the Eastern Alps it generally strikes east-west, it forms a system of SW-NE striking fault zones to the SW of the Tauern Window (Fig. 1). Some of the SW-NE striking faults even cross-cut the E-W trending faults. East of the Tauern Window, three major fault zones were active during Miocene lateral extrusion: the Mur-Mürz Fault, the Pöls-Lavanttal Fault and the Palten-Liesingtal-Fault (Fig. 1). The Mur-Mürz Fault can be separated into two segments. The western segment originates near the Katschberg normal fault and extends to the Miocene Fohnsdorf basin (Fig. 1). The eastern segment is located east of the Fohnsdorf basin and terminates underneath the Vienna basin (e.g. Ratschbacher et al., 1991b). The NNW-trending dextral Pöls-Lavanttal Fault separates the basement complexes of the Kor- and Saualm (Reinecker, 2000), and the Görtsch Valley Fault borders the Saualm to the west (Caporali et al., 2013). The Pöls-Lavanttal is assumed to have been active since Early Miocene times (Reinecker, 2000; Wöfler et al., 2010). Little is known about the role of the Palten-Liesingtal Fault during la-

teral extrusion. It strikes NW-SE with a minimal dextral offset of ~8 km (Linzer et al., 2002).

3.1 GEOLOGY OF THE EASTERN GREYWACKE ZONE

Tollmann (1977) subdivided the Austroalpine Nappe stack into a Lower, Middle and Upper Austroalpine Nappe Complex. By contrast Schuster and Frank (1999) and Schmid et al. (2004) divide the Austroalpine nappe stack according to their position with respect to the 90 Ma old high pressure wedge represented by the Koralpe Wölz nappe system. In both interpretations the Greywacke Zone and the overlying NCA occupy a high tectonic position and are therefore referred to as Upper Austroalpine nappes. The basement of the Upper Austroalpine is formed generally by low grade Palaeozoic metasedimentary units (Handler et al., 1997). These low grade Palaeozoic metasedimentary units are the Graz Nappe complex, the Gurktal Nappe complex and the Greywackezone. They are the oldest sedimentary units of the Upper Austroalpine units in the Eastern Alps with Ordovician to Carboniferous depositional ages.

The Greywackezone is generally divided into a western and an eastern part. The latter reaches from the eastern end of

Tectonic units

Stratigraphic units

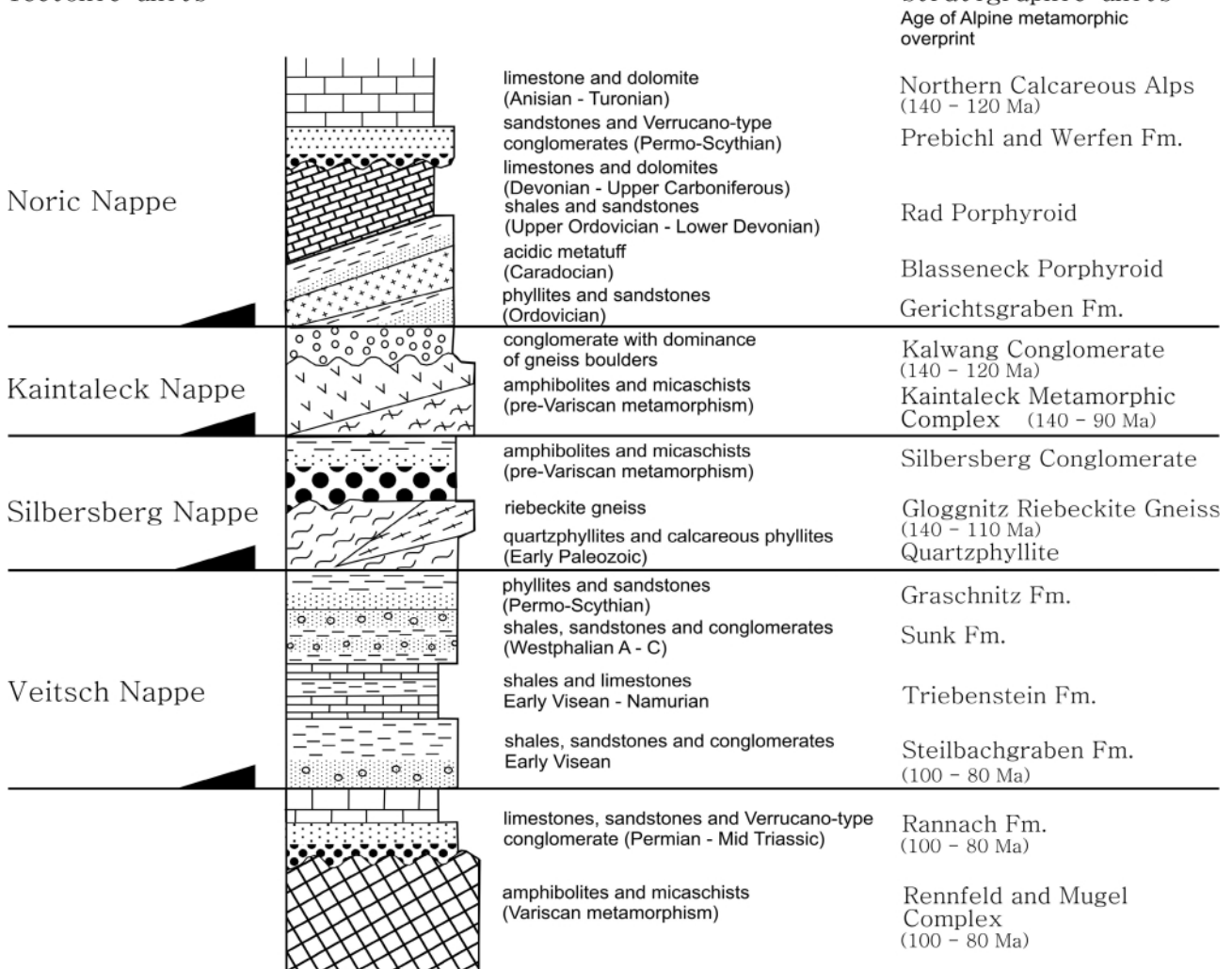


FIGURE 3: Stratigraphy of the Eastern Greywacke zone. Modified after Neubauer et al. (1994).

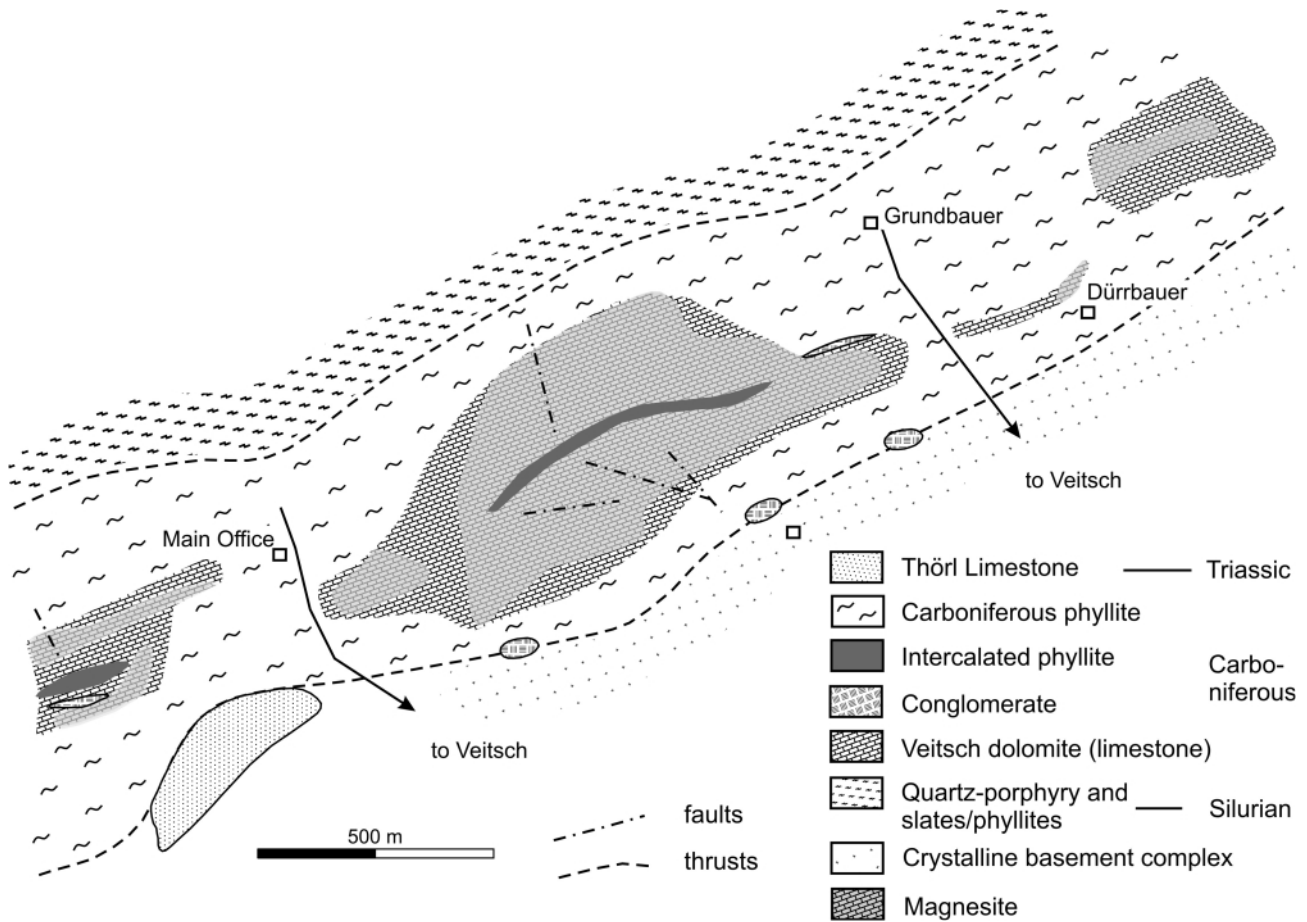


FIGURE 4: Geological sketch of the Veitsch magnesite deposit. Modified after Polgári et al. (2010).

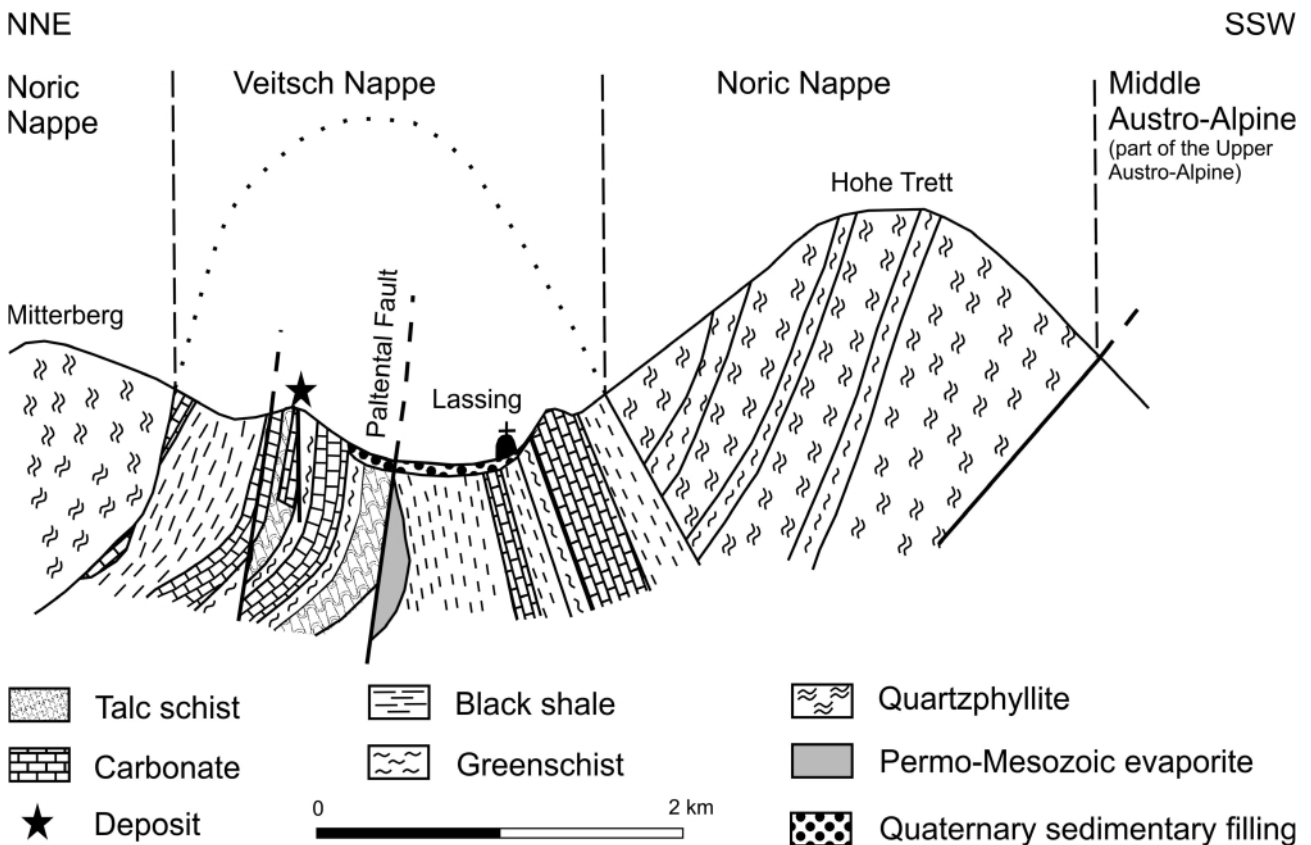


FIGURE 5: Geological sketch of the Lassing talc deposit. Modified after Prochaska (1989).

the Tauern Window to the Vienna Basin (Fig. 1 and 2). The rock series comprises Paleozoic carbonates, metapelites and acid volcanics and are of Ordovician ages.

The eastern Greywackezone comprises four nappe sheets from footwall to hangingwall: Veitsch nappe, Silbersberg nappe, Kaintaleck nappe and Noric nappe (Neubauer et al., 1993; Fig. 3).

The Veitsch nappe is composed of Carboniferous marine to deltaic carbonates and clastic sediments (Ratschbacher, 1987) however, the source area of these sediments still remains unknown (e.g. Schoenlaub, 1981; Ratschbacher, 1987; Ratschbacher and Frisch, 1993; Handler et al., 1997; Neubauer et al., 2002).

The Veitsch nappe is subdivided into three formations from footwall to hangingwall: Steilbachgraben Formation with clastics and minor carbonates, the Triebenstein Formation mainly composed of carbonates and few greenschists lenses, and the Sunk Formation containing quartz conglomerates and anthracite/graphite deposits (Neubauer et al., 1994). Lenses of magnesite are bound to marine carbonates of Visean age. Along shear zones small (e.g. cm to dm in scale at Wald am

Schober) to large talc accumulation (meter scale at Lassing) can be found.

The Silbersberg nappe consists of chloritecarbonate schists and quartzphyllite with intercalated lenses of foliated volcanics at the base of the nappe. Above a fine-grained mylonitic gneiss – the Gloggnitz Riebeckite Gneiss - forms the boundary to the Silbersberg Conglomerate containing light-colored greenish quartzitic phyllites with thin layers of acidic tuffs (Neubauer et al., 1993).

The Kaintaleck nappe is made of two lithological units: the Kaintaleck Metamorphic complex at the base of the nappe with amphibolites, paragneiss and micaschist as well as thin marble layers and lenses. The overlying Kalwang Conglomerate contains basement fragments as amphibolites and serpentinites but is mostly dominated by orthogneiss clasts.

Finally, the Noric Nappe is composed of Ordovician to Lower Carboniferous sediments i.e. arkosic phyllites (Gerichtsgraben-formation) at the base and overlain by the Blasseneck porphyroid and the Rad Phyllite made of slates and phyllites and is concluded with an angular unconformity that forms the boundary to the Prebichl Formation (Neubauer et al., 1993).

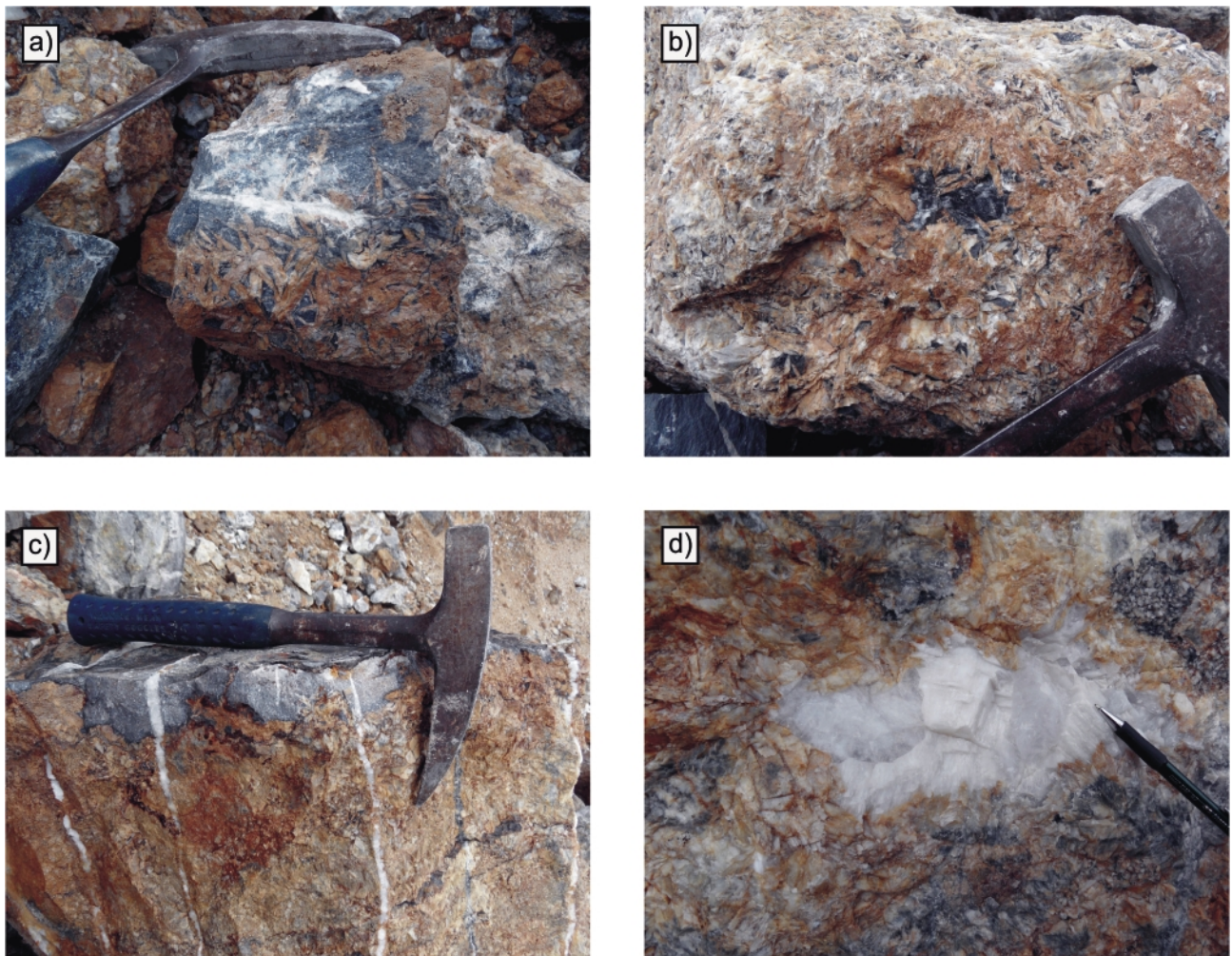


FIGURE 6: Field observations from the Veitsch magnesite deposit: a) Early state of magnesite formation from greyish precursor dolomite, b) Late state of magnesite formation with small residual precursor dolomite, c) Late dolomite veins penetrating magnesite and dolomite body, d) Late dolomite and quartz formation within magnesite.

3.2 GEOLOGY OF MAGNESITE DEPOSITS OF THE EASTERN GREYWACKE ZONE

The magnesite deposit in Veitsch represents the type locality for sparry magnesite. It is situated north of the village Veitsch in Styria and approximately 7 km from the valley floor of the Mürztal that forms the topographic expression of the Mur-Mürz-Fault (Fig.2). The magnesite body of the Veitsch deposit is hosted by dolomitic carbonate of Carboniferous age of the Veitsch nappe and also by Carboniferous calcite marbles, phyllites, meta-conglomerates, quarzites and meta-sandstones (Prochaska, 2000). The lense shaped magnesite bodies seem to evolve from the dolomitic carbonate. The carbonate bodies are embedded into Carboniferous phyllites and overlain by Ordovician quartz porphyry and phyllites/slates (Fig. 4). Within the magnesite bodies horsetooth dolomite occurs as well as abundant quartz veins that crosscut both the dolomitic carbonate and the magnesite. The magnesite body itself is coarsely grained with pinolitic and rosulate textures.

The magnesite deposit Wald am Schober is situated near the village of Wald am Schoberpass in Styria (Fig 2). It is only a couple of meters to the southwest above the valley floor of the Paltental and thus in close proximity to the Paltental-Liesingtal-Fault. The deposit is embedded in Carboniferous limestones (Felser, 1977) as part of the Veitsch nappe. The magnesite body is bordered by a broad rim of dolomite that smoothly passes into the magnesite body. At the bottom of the deposit bedded and massive limestones of Visean age occur. The magnesite body itself ranges from fine grained to coarsely grained magnesite and pinolitic sparry magnesite. Also horsetooth dolomite occurs within the magnesite body. An important feature of the Wald am Schober magnesite deposit is the occurrence of small to several cm – dm broad shear zones with talc and chlorite mineralization. In addition talc mineralizations also occur dispersely distributed within

the magnesite body. The magnesite body is overlain by dolomite as well as phyllites/slates and sandstone.

The talc deposit of Lassing has been abandoned since the cavern accident in 1998. It is situated at the junction of the SEMP and Paltental-Liesingtal Fault. The vein type talc mineralization is hosted by dolomitic carbonates of the Veitsch nappe. The rock succession of the deposit consist of lime-stones, dolomites, magnesite, clastic metasediments and subordinate basic metavolcanics of upper Visean and Namurian age (Prochaska, 1989). The talc deposit is situated along a major fault zone and to the north there is an E-W striking antiform of Carboniferous rocks that is cut by a wide strike-slip fault. It is flanked to the south by the Paltental-Liesing fault and to the north by a thrust zone (Prochaska, 1989), Fig. 5).

4 RESULTS

4.1 SAMPLE DESCRIPTION

The chosen deposits of the Eastern Greywackezone are hosted in similar lithologies with varying talc content. Only in the Lassing mine, talc was produced and occurs within dolomite hostrocks. The magnesite deposits of Veitsch and Wald am Schober produced magnesite while Wald am Schober contains talc impurities on a cm to dm scale within shear zones and dispersely accumulated within magnesite rocks.

The sparry magnesite body of the Veitsch deposit is generally of massive nature and contains mostly brittle deformation structures such as brittle faults or feather joints. The magnesite samples are of reddish color and coarsely grained. They evolve from a greyish dolomite hostrock. Both are part of the Veitsch nappe. The states of formation - the beginning of magnesite formation and the final state with an almost completely mineralized magnesite and only residual dolomite ("early state dolomite") - can be observed in the deposit (Fig. 6). Post-magnesite-formation veins of quartz and dolomite penetrate the dolomite and magnesite bodies. A sketch of the order of mineralization is shown in Fig. 7. Minor components of ore minerals as fahlore and malchite can be observed as well. Thus the evolution of the deposit can be reconstructed as follows: greyish precursor dolomite which evolves into a reddish sparry magnesite. Both are later penetrated by quartz and dolomite veins. The dolomite and quartz veins dip NNE with approx. 020/70 and NNW with approx. 340/45. A younger set of veins dips NE with approx. 305/80.

The magnesite deposit of Wald am Schober is clearly penetrated by ductile deformation. Structures as SC fabrics (Fig. 8c), shearzones (Fig. 8 a, b) and boundinages (Fig. 8 d) can be found. Shearzones are filled with talc mineralizations. Talc accumulations can be concentrated in the fault core of a shearzone (Fig. 8 f) or dispersely distributed within the magnesite body (Fig. 8 e). The sparry magnesite body itself is mostly of whitish or greyish color and coarsely grained and is part of the Veitsch nappe. Towards the shear zones it takes a reddish color and marks a seam along the shearzone. Talc mineralization within the shearzones are mostly of greyish and whitish

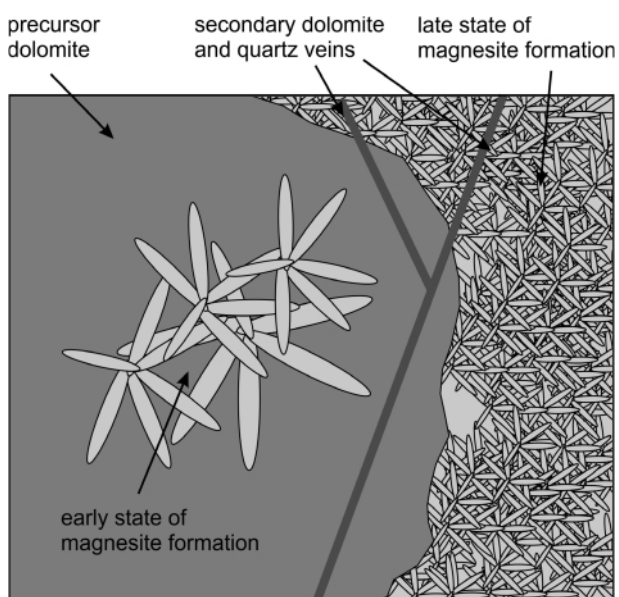


FIGURE 7: Sketch of mineralization phases at the Veitsch magnesite deposit.

color. More massive talc bodies (up to dm scale) are of milky whitish and yellowish color. Secondary carbonates such as the so called "horse tooth dolomite" also occur within the magnesite body. A sketch of the mineralization phases is shown in Fig. 9. Thin-sections confirm dispersely accumulated talc concentrations within the magnesite body (Fig. 10a). Shear zones are composed of a fine grained hyaline matrix of gouge material and fragments of carbonate rocks (Fig. 10b, c and d). The transition zone towards the hostrock magnesite body is marked by fractured carbonate rocks filled with a fine grained matrix (Fig. 10b).

The talc shearzones have a general dip of ESE with approx.

100/35 and WNW with approx. 330/20. Slickensides show normal faulting with approx. 100/35 and 330/20. A prominent fault approx. parallel to the Paltental-Liesingtal-fault dips NNE with approx. 010/60 and reveals two generations of slickenside with dextral sense of shear and 308/15 for the younger one and 020/60 for the older one with a normal faulting component.

The talc deposit of Lassing has been closed since the mining disaster in 1998. Hence samples could only be taken from surface exposures. Some handspecimen from the deposit were available at the University of Leoben and could be used for analysis. The massive talc mineralization lies within a dolomite body that is part of the Veitsch nappe.

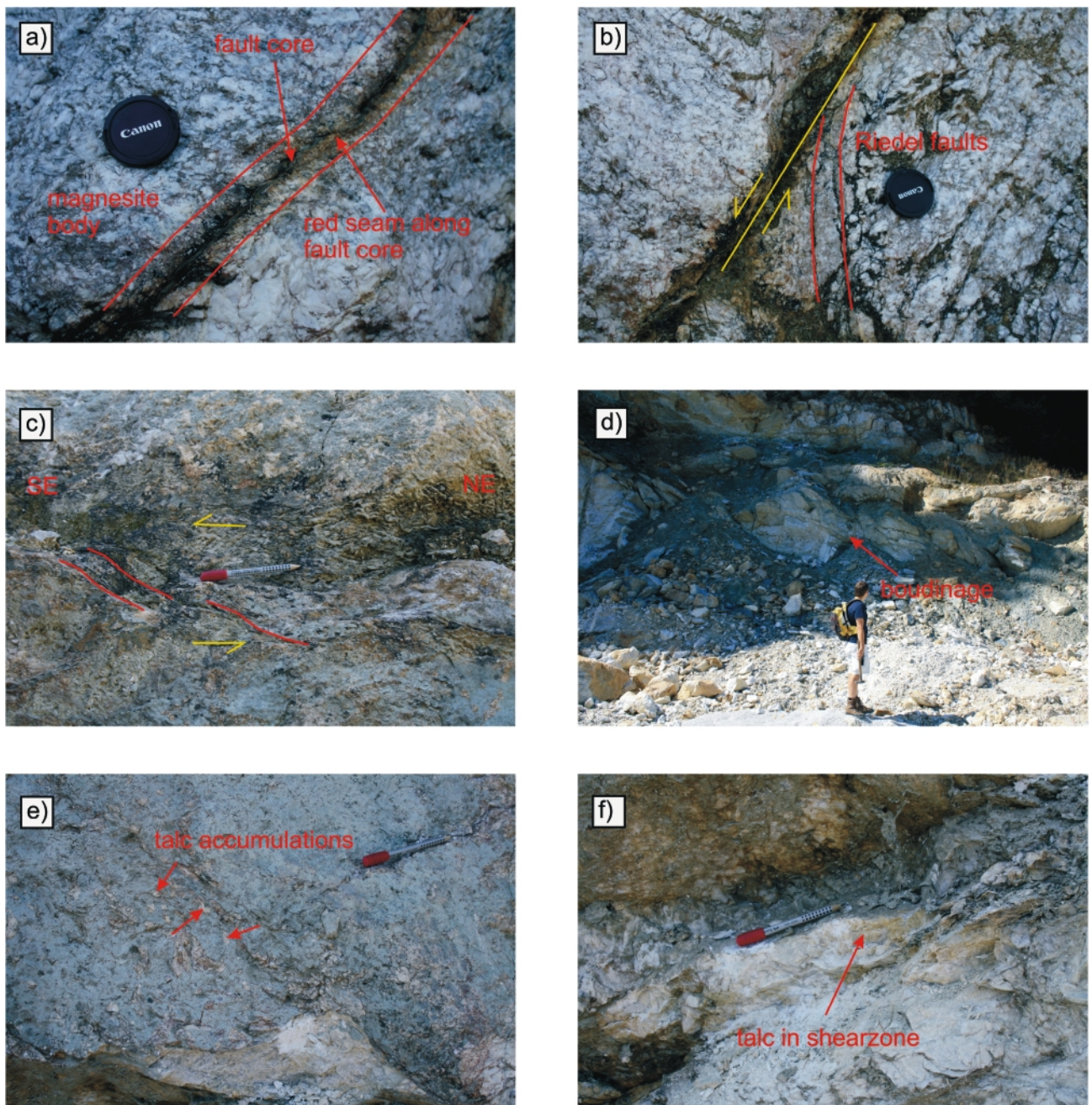


FIGURE 8: Field observations from the Wald am Schober magnesite deposit: a) shear zone with talc fault core and reddish seam along the fault core within magnesite body, b) shear zone with horsetails indicating normal sense of shear, c) shear zone with SC texture indicating sinistral sense of shear, d) boudinage, e) dispersely distributed talc accumulations within magnesite body, f) larger talc accumulation in shearzone.

Thin-sections from the surroundings of the Lassing talc mine reveal multiple deformation events that overprinted the carbo-

nate rocks (Fig. 11a). Younger quartz veins within these rocks show also signs of deformation such as undulose extinction and bulging (Fig. 11b).

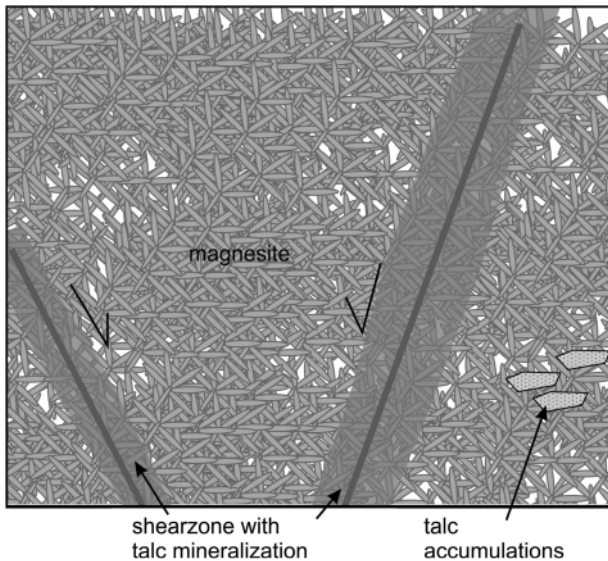


FIGURE 9: Sketch of the mineralization phases at the Wald am Schober magnesite deposit.

4.2 MAJOR, MINOR, TRACE ELEMENTS

Rock samples from each deposit were analyzed with regard to the tectonic structures in the respective deposits (Tab. 1-3).

In the Veitsch deposit samples from the magnesite, the precursor dolomite and the vein mineralizations were analyzed. Magnesite samples (VE5a, VE14b) are slightly depleted in MgO (36.77 - 43.22 wt%) (compared to values of magnesite from Deer et al., 1992) and elevated in CaO (2.24 - 8.17 wt%), FeO (3.55 - 4.82 wt%) and Sr (27 - 63 ppm). Other minor and trace elements analyzed do not give hints on significant elevation or depletion of the magnesite. The dolomites of the deposit seem to be dividable into two groups. Such grey dolomites with no intermediate contact to magnesite (VE7, VE9, VE14a) have partly a different geochemical composition than dolomites that are in direct contact with magnesite (VE2a, VE2b, VE5b, VE5c, VE5d). The latter represent more the late state of magnesite mineralization. Major and minor element composition of both dolomite groups are comparable and do

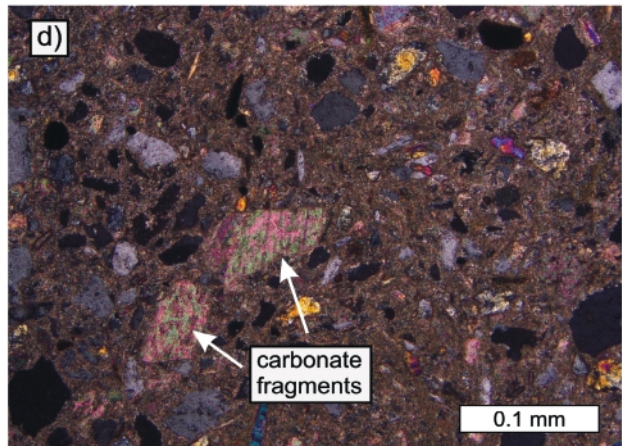
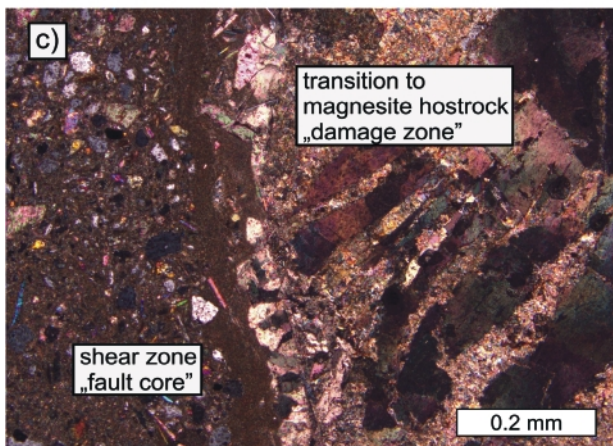
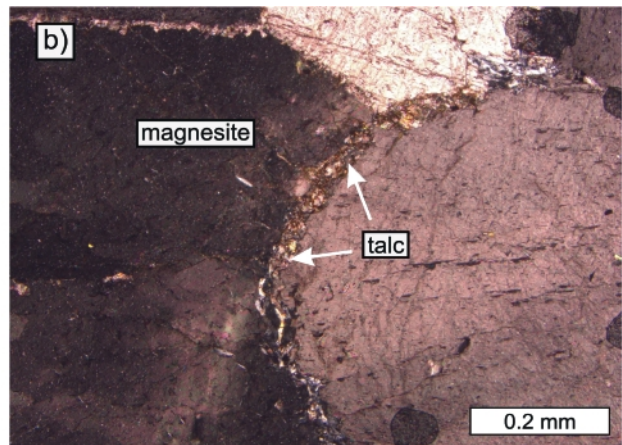
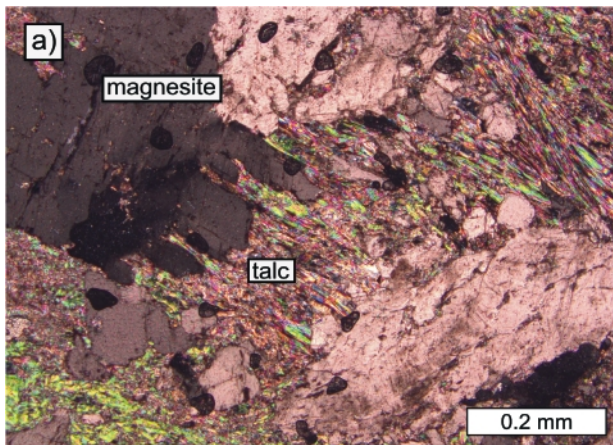


FIGURE 10: Thin-sections of the Wald am Schober magnesite deposit: a) and b) the magnesite body is penetrated by disperse talc accumulations, c) the shear zones of the deposit consist of a fined grained hyaline matrix of gouge material with fragments of carbonate; the transition zone towards the magnesite hostrock body shows broken carbonate grains filled with a fine grained matrix, d) carbonate fragments within a hyaline matrix of gouge material.

Sample Rocktype remarks	VE 2a dol vein	VE 7 dol marble	VE 9 dol marble	VE 14a dol marble	VE 14b mgs	VE 2b dol vein	VE 5c dol vein	VE 5b dol vein	VE 5d dol vein	VE 5a mgs	SU 1 cc marble hostrock	SU 2 cc marble hostrock	WS 7 dol marble hostrock	WS 8 dol marble hostrock
wt%														
SiO ₂	1.73	1.47	0.73	1.4	2.5	2.15	0.13	0.18	0.76	0.28	2.32	1.44	4.58	2.15
Al ₂ O ₃	1.15	0.26	0.41	0.77	0.79	0.24	0.03	0.07	0.05	0.16	0.53	0.16	0.07	0.13
Fe ₂ O ₃ (T)	3	0.98	1.27	1.35	4.82	1.64	1.63	2.75	2.47	3.55	0.4	0.17	0.12	0.4
MnO	0.156	0.124	0.16	0.102	0.243	0.124	0.132	0.186	0.168	0.223	0.014	0.036	0.019	0.033
MgO	28.34	21.42	21.57	21.79	36.77	20.28	20.88	19.5	20.14	43.22	0.66	0.53	20.22	20.8
CaO	20.34	30.2	30.33	29.3	8.17	29.24	30.47	30.03	29.96	2.24	52.52	54.41	28.98	29.83
Na ₂ O	0.03	0.06	0.07	0.06	0.04	0.08	0.02	0.03	0.04	0.02	0.07	0.07	0.03	0.03
K ₂ O	< 0.01	< 0.01	0.01	0.01	< 0.01	0.02	< 0.01	< 0.01	< 0.01	< 0.01	0.1	0.03	< 0.01	< 0.01
TiO ₂	0.096	0.006	0.01	0.016	0.027	0.002	< 0.001	0.002	< 0.001	0.004	0.022	0.004	0.003	0.01
P ₂ O ₅	0.02	0.04	0.05	0.04	0.07	0.04	< 0.01	0.03	0.02	0.05	0.03	0.02	0.06	0.11
LOI	45.77	46.27	46.38	45.79	47.17	45.71	46.94	46.41	46.21	50.35	42.93	44.1	44.43	46
Total	100.6	100.8	101	100.6	100.6	99.53	100.2	99.19	99.83	100.1	99.61	101	98.52	99.5
ppm														
Sc	2	< 1	1	1	1	1	1	2	2	< 1	1	< 1	< 1	< 1
Be	< 1	< 1	< 1	< 1	< 1	< 1	< 1	< 1	< 1	< 1	< 1	< 1	< 1	< 1
V	23	17	18	15	16	15	12	10	12	8	11	8	11	15
Cr	< 20	< 20	< 20	< 20	< 20	< 20	< 20	< 20	< 20	< 20	< 20	< 20	< 20	< 20
Co	8	< 1	< 1	1	5	< 1	< 1	< 1	< 1	2	6	8	< 1	< 1
Ni	30	< 20	< 20	< 20	< 20	< 20	< 20	< 20	< 20	< 20	< 20	< 20	< 20	< 20
Cu	< 10	< 10	< 10	< 10	20	< 10	< 10	< 10	< 10	30	10	10	< 10	< 10
Zn	< 30	< 30	< 30	< 30	< 30	< 30	< 30	50	< 30	< 30	< 30	< 30	< 30	< 30
Ga	2	< 1	< 1	1	1	< 1	< 1	< 1	< 1	< 1	< 1	< 1	< 1	< 1
Ge	< 0.5	< 0.5	< 0.5	< 0.5	< 0.5	< 0.5	< 0.5	< 0.5	< 0.5	< 0.5	< 0.5	< 0.5	< 0.5	< 0.5
As	43	< 5	8	16	22	< 5	< 5	< 5	< 5	12	< 5	< 5	< 5	< 5
Rb	< 1	< 1	< 1	< 1	< 1	< 1	< 1	< 1	< 1	< 1	4	< 1	< 1	< 1
Sr	246	51	32	77	63	334	308	233	260	27	336	720	116	119
Y	5.9	1.2	2	5	7.7	14	7.5	27.4	20.7	3.4	9.5	2.5	< 0.5	0.6
Zr	22	2	3	3	6	< 1	3	< 1	4	2	6	2	< 1	2
Nb	1.9	< 0.2	< 0.2	< 0.2	< 0.2	< 0.2	< 0.2	< 0.2	< 0.2	< 0.2	0.4	< 0.2	< 0.2	< 0.2
Mo	< 2	< 2	< 2	< 2	< 2	< 2	< 2	< 2	< 2	< 2	< 2	< 2	< 2	< 2
Ag	< 0.5	< 0.5	< 0.5	< 0.5	< 0.5	< 0.5	< 0.5	< 0.5	< 0.5	< 0.5	< 0.5	< 0.5	< 0.5	< 0.5
In	< 0.1	< 0.1	< 0.1	< 0.1	< 0.1	< 0.1	< 0.1	< 0.1	< 0.1	< 0.1	< 0.1	< 0.1	< 0.1	< 0.1
Sn	< 1	< 1	< 1	< 1	< 1	< 1	< 1	< 1	< 1	< 1	< 1	< 1	< 1	< 1
Sb	2.7	< 0.2	0.9	< 0.2	2.7	< 0.2	< 0.2	0.6	0.2	6.6	< 0.2	0.7	< 0.2	< 0.2
Cs	< 0.1	< 0.1	< 0.1	< 0.1	< 0.1	< 0.1	< 0.1	< 0.1	< 0.1	< 0.1	0.1	< 0.1	< 0.1	< 0.1
Ba	< 3	< 3	3	< 3	5	< 3	< 3	< 3	< 3	< 3	19	7	< 3	< 3
Hf	0.5	< 0.1	< 0.1	< 0.1	0.1	< 0.1	< 0.1	< 0.1	0.2	< 0.1	0.1	< 0.1	< 0.1	< 0.1
Ta	0.11	< 0.01	< 0.01	< 0.01	< 0.01	< 0.01	< 0.01	< 0.01	< 0.01	< 0.01	0.02	< 0.01	< 0.01	< 0.01
W	< 0.5	< 0.5	< 0.5	< 0.5	< 0.5	2.3	1.1	< 0.5	< 0.5	< 0.5	< 0.5	6.4	< 0.5	< 0.5
Tl	< 0.05	< 0.05	< 0.05	< 0.05	< 0.05	< 0.05	< 0.05	< 0.05	< 0.05	< 0.05	< 0.05	< 0.05	< 0.05	< 0.05
Pb	5	< 5	< 5	< 5	< 5	< 5	< 5	< 5	< 5	< 5	< 5	< 5	< 5	< 5
Bi	1.4	< 0.1	0.9	0.5	1.5	< 0.1	< 0.1	< 0.1	< 0.1	0.2	0.3	< 0.1	< 0.1	< 0.1
Th	1.79	0.18	0.23	0.44	0.43	< 0.05	< 0.05	< 0.05	0.06	0.13	0.6	0.14	< 0.05	0.13
U	2.42	0.75	1.38	1.12	1.33	0.11	0.19	0.18	0.23	1.04	0.94	8.41	0.51	2.62
La	7.28	1.35	1.41	0.97	1.32	6.67	13.2	7.97	8.14	0.67	5.16	1.33	0.48	0.56
Ce	11.7	2.46	2.56	2.45	3.84	15.6	24.2	20.3	18.1	2.06	7.1	1.73	0.8	1.21
Pr	1.37	0.3	0.33	0.43	0.54	2.18	2.61	2.76	2.41	0.4	1.08	0.22	0.1	0.15
Nd	5.71	1.32	1.52	2.43	2.86	9.3	9.86	12.5	10.2	2.23	4.65	0.9	0.4	0.66
Sm	1.61	0.28	0.37	1.48	1.92	2.58	1.86	3.61	2.8	1.01	1.05	0.17	0.08	0.14
Eu	1.39	0.13	0.141	0.531	0.756	1.14	0.895	0.696	0.712	0.5	0.228	0.043	0.021	0.083
Gd	1.5	0.3	0.36	1.7	2.49	2.52	1.7	3.67	2.78	1.05	1.16	0.24	0.07	0.14
Tb	0.21	0.04	0.06	0.23	0.36	0.39	0.22	0.66	0.51	0.13	0.18	0.04	0.01	0.02
Dy	1.07	0.19	0.34	1.13	1.75	2.27	1.3	4.58	3.28	0.59	1.17	0.26	0.07	0.12
Ho	0.2	0.04	0.07	0.18	0.27	0.42	0.23	0.92	0.65	0.1	0.26	0.06	0.01	0.02
Er	0.56	0.11	0.21	0.44	0.64	1.19	0.68	2.84	1.98	0.25	0.72	0.18	0.04	0.05
Tm	0.084	0.016	0.031	0.051	0.083	0.154	0.102	0.427	0.297	0.033	0.103	0.028	< 0.005	0.008
Yb	0.56	0.1	0.19	0.3	0.44	0.96	0.67	2.65	1.86	0.2	0.65	0.19	0.04	0.05
Lu	0.079	0.015	0.034	0.044	0.068	0.127	0.099	0.419	0.277	0.031	0.105	0.032	0.006	0.008

TABLE 1: Major, minor and trace elements from Veitsch (VE) and surrounding hostrocks (SU1, SU2, WS7, WS8)

Shear zone related talc mineralizations in the Veitsch nappe of the eastern Greywacke Zone (Eastern Alps, Austria)

Sample Rocktype remarks	WS 12 mgs talc	WS 9c a mgs shearzone	WS 9c b mgs shearzone	WS 10b a mgs shearzone	WS 1 dol vein	WS 2 mgs no talc	WS 3 mgs talc	WS 4 mgs no talc	WS 9b d mgs no talc	WS 9b h mgs no talc	WS 9b g mgs shearzone	WS 11 mgs talc	WS 20 mgs talc	WS 21 mgs talc
wt%														
SiO ₂	4.94	1.86	1.65	1.76	0.24	4.98	2.82	1.47	1.06	1.17	1.78	5.93	14.05	2.89
Al ₂ O ₃	0.36	0.25	0.21	0.33	0.1	0.38	0.08	0.09	0.09	0.09	0.11	0.12	1.08	0.02
Fe ₂ O ₃ (T)	1.22	1.22	1.29	1.25	0.54	1.48	1.65	1.57	1.26	1.31	1.29	1.21	2.1	1.65
MnO	0.081	0.077	0.08	0.085	0.037	0.076	0.096	0.091	0.079	0.08	0.08	0.074	0.079	0.104
MgO	45.53	42.85	44.64	45.97	21.28	45.71	45.59	46.52	46.35	46.9	45.87	45.83	38.58	45.91
CaO	0.69	5.02	2.63	0.7	30.03	0.5	0.59	0.67	1.11	0.44	1.35	0.62	4.76	0.56
Na ₂ O	0.05	0.03	0.05	0.06	0.04	0.02	0.03	0.03	0.05	0.04	0.03	0.02	0.03	0.03
K ₂ O	0.02	< 0.01	0.01	0.02	< 0.01	< 0.01	< 0.01	< 0.01	< 0.01	< 0.01	< 0.01	< 0.01	< 0.01	< 0.01
TiO ₂	0.032	0.009	0.005	0.024	< 0.001	0.031	0.004	0.006	0.002	0.002	0.004	0.013	0.118	0.002
P ₂ O ₅	< 0.01	< 0.01	0.03	0.04	0.02	0.02	0.04	< 0.01	0.03	0.02	0.02	0.01	0.03	0.01
LOI	47.89	49.58	50.14	50.11	47.05	47.65	49.37	50.49	50.86	50.88	50.17	47.1	39.72	49.57
Total	100.8	100.9	100.7	100.4	99.34	100.8	100.3	100.9	100.9	100.9	100.7	100.9	100.5	100.7
ppm														
Sc	< 1	< 1	< 1	3	6	1	< 1	< 1	< 1	< 1	< 1	< 1	6	< 1
Be	< 1	< 1	< 1	< 1	< 1	< 1	< 1	< 1	< 1	< 1	< 1	< 1	< 1	< 1
V	30	15	18	16	14	20	20	24	19	17	13	17	76	18
Cr	< 20	< 20	< 20	< 20	< 20	< 20	< 20	< 20	< 20	< 20	< 20	< 20	< 20	< 20
Co	< 1	< 1	< 1	< 1	< 1	< 1	< 1	< 1	< 1	< 1	< 1	< 1	< 1	< 1
Ni	< 20	< 20	< 20	< 20	< 20	< 20	< 20	< 20	< 20	< 20	< 20	< 20	< 20	< 20
Cu	< 10	< 10	< 10	< 10	< 10	< 10	< 10	< 10	< 10	< 10	< 10	< 10	< 10	< 10
Zn	< 30	< 30	< 30	< 30	< 30	< 30	< 30	< 30	< 30	< 30	< 30	< 30	< 30	< 30
Ga	< 1	< 1	< 1	< 1	< 1	< 1	< 1	< 1	< 1	< 1	< 1	< 1	2	< 1
Ge	< 0.5	< 0.5	< 0.5	< 0.5	< 0.5	< 0.5	< 0.5	< 0.5	< 0.5	< 0.5	< 0.5	< 0.5	1.3	< 0.5
As	< 5	< 5	< 5	< 5	< 5	< 5	< 5	< 5	< 5	< 5	< 5	< 5	< 5	< 5
Rb	< 1	< 1	< 1	< 1	< 1	< 1	< 1	< 1	< 1	< 1	< 1	< 1	< 1	< 1
Sr	4	29	19	4	65	< 2	2	3	4	3	5	4	46	3
Y	1	2.8	2.2	2.2	11.4	3.3	1.6	1.1	2.2	2	2	1	6.2	6.4
Zr	3	2	1	2	< 1	5	< 1	1	< 1	< 1	1	2	9	< 1
Nb	< 0.2	< 0.2	< 0.2	< 0.2	< 0.2	< 0.2	< 0.2	< 0.2	< 0.2	< 0.2	< 0.2	< 0.2	< 0.2	< 0.2
Mo	< 2	< 2	< 2	< 2	< 2	< 2	< 2	< 2	< 2	< 2	< 2	< 2	< 2	< 2
Ag	< 0.5	< 0.5	< 0.5	< 0.5	< 0.5	< 0.5	< 0.5	< 0.5	< 0.5	< 0.5	< 0.5	< 0.5	< 0.5	< 0.5
In	< 0.1	< 0.1	< 0.1	< 0.1	< 0.1	< 0.1	< 0.1	< 0.1	< 0.1	< 0.1	< 0.1	< 0.1	< 0.1	< 0.1
Sn	< 1	< 1	< 1	< 1	< 1	< 1	< 1	< 1	< 1	< 1	< 1	< 1	< 1	< 1
Sb	< 0.2	< 0.2	< 0.2	< 0.2	0.2	< 0.2	< 0.2	< 0.2	< 0.2	< 0.2	< 0.2	< 0.2	0.6	< 0.2
Cs	< 0.1	< 0.1	< 0.1	< 0.1	< 0.1	< 0.1	< 0.1	< 0.1	< 0.1	< 0.1	< 0.1	< 0.1	< 0.1	< 0.1
Ba	< 3	< 3	< 3	< 3	< 3	< 3	< 3	< 3	< 3	< 3	< 3	< 3	< 3	< 3
Hf	< 0.1	< 0.1	< 0.1	< 0.1	< 0.1	0.1	< 0.1	< 0.1	< 0.1	< 0.1	< 0.1	< 0.1	0.2	< 0.1
Ta	< 0.01	< 0.01	< 0.01	< 0.01	< 0.01	< 0.01	< 0.01	< 0.01	< 0.01	< 0.01	< 0.01	< 0.01	0.01	< 0.01
W	< 0.5	< 0.5	< 0.5	< 0.5	< 0.5	< 0.5	< 0.5	< 0.5	< 0.5	< 0.5	< 0.5	< 0.5	< 0.5	< 0.5
Tl	< 0.05	< 0.05	< 0.05	< 0.05	< 0.05	< 0.05	< 0.05	< 0.05	< 0.05	< 0.05	< 0.05	< 0.05	< 0.05	< 0.05
Pb	< 5	< 5	< 5	< 5	< 5	< 5	< 5	< 5	< 5	< 5	< 5	< 5	< 5	< 5
Bi	< 0.1	< 0.1	< 0.1	< 0.1	< 0.1	< 0.1	< 0.1	< 0.1	< 0.1	< 0.1	< 0.1	< 0.1	< 0.1	0.2
Th	0.17	0.14	0.09	0.05	< 0.05	0.17	< 0.05	< 0.05	< 0.05	0.06	0.08	0.06	0.31	< 0.05
U	0.26	0.28	0.22	0.21	0.03	0.2	0.07	0.09	0.19	0.28	0.22	0.18	0.17	0.02
La	0.56	0.45	0.36	0.34	1.22	0.37	0.57	0.45	0.19	0.15	0.17	0.16	0.32	0.22
Ce	1.49	1.66	1.27	1.08	9.21	1.36	2.15	2	0.56	0.41	0.48	0.61	0.93	0.73
Pr	0.26	0.35	0.26	0.22	2.28	0.28	0.4	0.39	0.12	0.08	0.1	0.13	0.19	0.18
Nd	1.66	2.44	1.89	1.5	15.9	1.65	2.23	2.08	0.8	0.62	0.77	0.91	1.53	1.42
Sm	1.03	1.38	1.06	0.81	8.45	0.74	0.88	0.65	0.63	0.45	0.52	0.46	1.21	1.41
Eu	0.342	0.391	0.295	0.213	3.69	0.327	0.442	0.406	0.126	0.103	0.12	0.157	0.401	0.514
Gd	0.77	1.34	1.1	0.76	7.58	0.82	0.9	0.52	0.64	0.59	0.67	0.37	1.58	2.02
Tb	0.06	0.14	0.11	0.08	0.79	0.11	0.08	0.05	0.09	0.08	0.09	0.04	0.24	0.28
Dy	0.26	0.64	0.53	0.41	3.41	0.62	0.33	0.24	0.45	0.41	0.43	0.21	1.37	1.44
Ho	0.04	0.1	0.09	0.08	0.46	0.11	0.05	0.04	0.08	0.07	0.07	0.04	0.25	0.23
Er	0.12	0.26	0.21	0.23	1.05	0.3	0.12	0.1	0.19	0.18	0.17	0.09	0.75	0.6
Tm	0.016	0.031	0.025	0.036	0.095	0.043	0.019	0.015	0.024	0.021	0.021	0.012	0.115	0.075
Yb	0.11	0.16	0.14	0.23	0.53	0.26	0.14	0.09	0.13	0.12	0.11	0.07	0.7	0.4
Lu	0.018	0.022	0.019	0.035	0.056	0.038	0.02	0.014	0.017	0.017	0.016	0.012	0.102	0.054

TABLE 2: Major, minor and trace elements from Wald am Schober (WS)

Sample Rocktype remarks	LA 2 cc marble	LA 4 cc marble	LA 1a dol marble	LA 8 cc marble	LA 12 cc marble	LA 9a cc marble	LA 9b cc marble	LA PR 31 dol marble	LA PR 33 mgs	LA PR 48 dol marble	LA PR 65 dol marble	LA PR 85 dol marble	LA PR 121 dol marble
wt%													
SiO ₂	6.64	3.94	1.38	3.73	1.61	4.48	5.24	7.54	3.3	10.94	6.86	18.27	1.7
Al ₂ O ₃	0.41	0.25	0.3	0.22	0.15	0.2	0.91	0.18	0.38	0.3	0.12	0.28	0.16
Fe ₂ O ₃ (T)	0.43	0.26	0.82	0.18	0.11	0.17	0.51	0.78	1.15	0.69	0.36	0.37	0.4
MnO	0.078	0.02	0.071	0.01	0.014	0.034	0.041	0.067	0.063	0.057	0.023	0.018	0.026
MgO	1.91	2.05	18.73	0.68	2.1	5.19	4.08	21.2	42.77	22.39	21.47	13.73	20.95
CaO	49.18	50.99	33.1	53.51	51.36	49.1	49.22	27.3	3.47	24.67	27.69	28.67	29.69
Na ₂ O	0.16	0.07	0.03	0.06	0.05	0.04	0.04	0.06	0.04	0.06	0.04	0.04	0.06
K ₂ O	0.08	0.04	0.05	0.06	0.05	0.01	0.01	0.01	< 0.01	0.02	< 0.01	< 0.01	0.02
TiO ₂	0.009	0.009	0.008	0.015	0.006	0.012	0.083	0.006	0.019	0.018	0.004	0.016	0.006
P ₂ O ₅	< 0.01	0.01	0.03	0.02	0.01	0.01	0.06	0.01	0.03	< 0.01	0.02	0.03	0.01
LOI	40.98	42.57	45.93	42.23	43.42	41.63	40.28	42.95	49.56	40.65	43.68	38.32	46.69
Total	99.88	100.2	100.4	100.7	98.88	100.9	100.5	100.1	100.8	99.8	100.3	99.76	99.72
ppm													
Sc	< 1	< 1	< 1	< 1	< 1	< 1	2	< 1	< 1	1	< 1	< 1	< 1
Be	< 1	< 1	< 1	< 1	< 1	< 1	< 1	< 1	< 1	< 1	< 1	< 1	< 1
V	8	6	13	8	14	9	20	6	16	8	10	7	< 5
Cr	< 20	< 20	< 20	< 20	< 20	< 20	< 20	< 20	< 20	< 20	< 20	< 20	< 20
Co	< 1	< 1	< 1	< 1	< 1	< 1	< 1	3	< 1	2	2	3	2
Ni	< 20	< 20	< 20	< 20	< 20	< 20	< 20	< 20	< 20	< 20	< 20	< 20	< 20
Cu	< 10	< 10	< 10	< 10	10	< 10	< 10	< 10	< 10	< 10	< 10	< 10	< 10
Zn	< 30	< 30	< 30	< 30	< 30	< 30	< 30	< 30	< 30	< 30	< 30	< 30	< 30
Ga	< 1	< 1	< 1	< 1	< 1	< 1	2	< 1	< 1	< 1	< 1	< 1	< 1
Ge	< 0.5	< 0.5	< 0.5	< 0.5	< 0.5	< 0.5	< 0.5	< 0.5	< 0.5	1	< 0.5	< 0.5	< 0.5
As	< 5	< 5	< 5	< 5	< 5	< 5	< 5	< 5	< 5	< 5	< 5	< 5	< 5
Rb	< 1	< 1	1	< 1	< 1	< 1	< 1	< 1	< 1	< 1	< 1	< 1	< 1
Sr	206	207	170	193	186	301	281	74	51	208	106	92	90
Y	3.2	1.6	1.7	1.2	< 0.5	1.2	6.2	< 0.5	1	3.4	0.7	0.7	< 0.5
Zr	22	11	2	5	1	2	31	1	4	2	1	2	2
Nb	< 0.2	< 0.2	0.5	< 0.2	< 0.2	0.3	2.7	< 0.2	0.4	0.2	< 0.2	< 0.2	< 0.2
Mo	< 2	< 2	< 2	< 2	< 2	< 2	< 2	< 2	< 2	< 2	< 2	< 2	< 2
Ag	< 0.5	< 0.5	< 0.5	< 0.5	< 0.5	< 0.5	< 0.5	< 0.5	< 0.5	< 0.5	< 0.5	< 0.5	< 0.5
In	< 0.1	< 0.1	< 0.1	< 0.1	< 0.1	< 0.1	< 0.1	< 0.1	< 0.1	< 0.1	< 0.1	< 0.1	< 0.1
Sn	< 1	< 1	< 1	< 1	< 1	< 1	< 1	< 1	< 1	< 1	1	< 1	2
Sb	< 0.2	< 0.2	0.2	< 0.2	< 0.2	< 0.2	< 0.2	0.7	0.7	0.6	0.9	< 0.2	< 0.2
Cs	< 0.1	< 0.1	< 0.1	< 0.1	< 0.1	< 0.1	< 0.1	< 0.1	< 0.1	0.1	< 0.1	< 0.1	< 0.1
Ba	7	7	15	6	6	6	5	4	< 3	3	43	< 3	< 3
Hf	0.8	0.3	< 0.1	0.1	< 0.1	< 0.1	0.8	< 0.1	0.1	< 0.1	< 0.1	< 0.1	< 0.1
Ta	< 0.01	< 0.01	< 0.01	< 0.01	< 0.01	0.02	0.17	< 0.01	0.05	0.03	0.03	0.02	0.04
W	17.5	< 0.5	< 0.5	< 0.5	< 0.5	< 0.5	< 0.5	< 0.5	< 0.5	< 0.5	< 0.5	< 0.5	< 0.5
Tl	< 0.05	< 0.05	< 0.05	< 0.05	< 0.05	0.07	< 0.05	< 0.05	< 0.05	< 0.05	< 0.05	< 0.05	< 0.05
Pb	< 5	< 5	< 5	< 5	< 5	< 5	< 5	< 5	< 5	< 5	< 5	< 5	< 5
Bi	< 0.1	< 0.1	0.2	< 0.1	< 0.1	< 0.1	< 0.1	< 0.1	< 0.1	< 0.1	< 0.1	< 0.1	< 0.1
Th	0.56	0.29	0.17	0.05	0.11	0.13	0.31	0.07	0.41	0.06	0.09	0.13	0.07
U	0.44	0.24	0.37	0.76	0.43	0.21	0.54	0.31	0.41	0.25	2.31	0.32	0.2
La	1.86	0.88	1.62	0.85	0.61	2.17	3.14	0.81	0.55	2.05	0.76	0.67	0.47
Ce	3.33	1.8	2.71	1.66	3.04	3.91	7.27	1.46	1.48	6.08	1.68	1.19	0.85
Pr	0.39	0.2	0.37	0.22	0.09	0.42	0.97	0.16	0.23	0.98	0.22	0.14	0.09
Nd	1.77	0.88	1.66	0.94	0.37	1.79	4.51	0.57	1.17	4.6	0.85	0.67	0.38
Sm	0.46	0.21	0.34	0.26	0.08	0.39	1.16	0.1	0.3	1.2	0.17	0.14	0.07
Eu	0.211	0.101	0.098	0.067	0.023	0.1	0.261	0.088	0.123	0.437	0.058	0.027	0.037
Gd	0.58	0.27	0.35	0.23	0.08	0.32	1.26	0.08	0.24	1.04	0.16	0.14	0.06
Tb	0.09	0.05	0.06	0.04	0.01	0.05	0.21	0.01	0.03	0.13	0.02	0.02	< 0.01
Dy	0.53	0.3	0.3	0.23	0.08	0.25	1.23	0.07	0.17	0.7	0.12	0.13	0.05
Ho	0.11	0.06	0.06	0.04	0.01	0.04	0.23	0.02	0.03	0.13	0.03	0.03	< 0.01
Er	0.33	0.18	0.16	0.12	0.03	0.12	0.69	0.05	0.1	0.34	0.08	0.08	0.03
Tm	0.05	0.028	0.023	0.017	0.006	0.015	0.096	0.008	0.015	0.045	0.01	0.013	< 0.005
Yb	0.31	0.18	0.15	0.11	0.04	0.08	0.62	0.05	0.09	0.24	0.06	0.08	0.03
Lu	0.055	0.025	0.025	0.018	0.006	0.012	0.098	0.007	0.015	0.036	0.01	0.014	0.005

TABLE 3: Major, minor and trace elements from inside the Lassing talc mine (LA-PR) and surrounding rocks (LA)

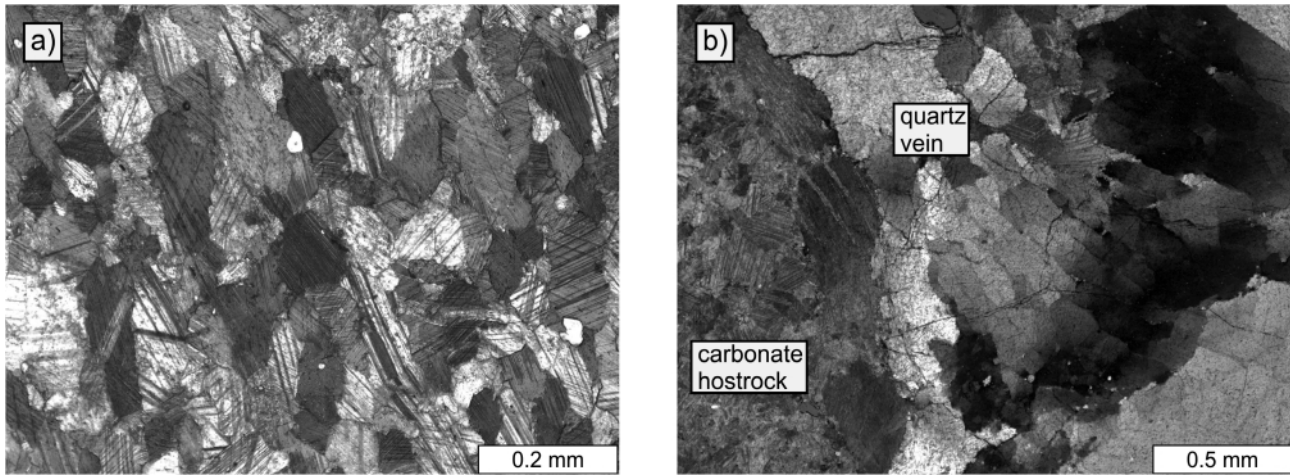


FIGURE 11: Thin-sections from the surroundings of the Lassing talc deposit: a) Calcitic marble shows multiple deformation events, b) Secondary quartz vein in calcitic marble c) statically grown late quartz grains within calcitic marble.

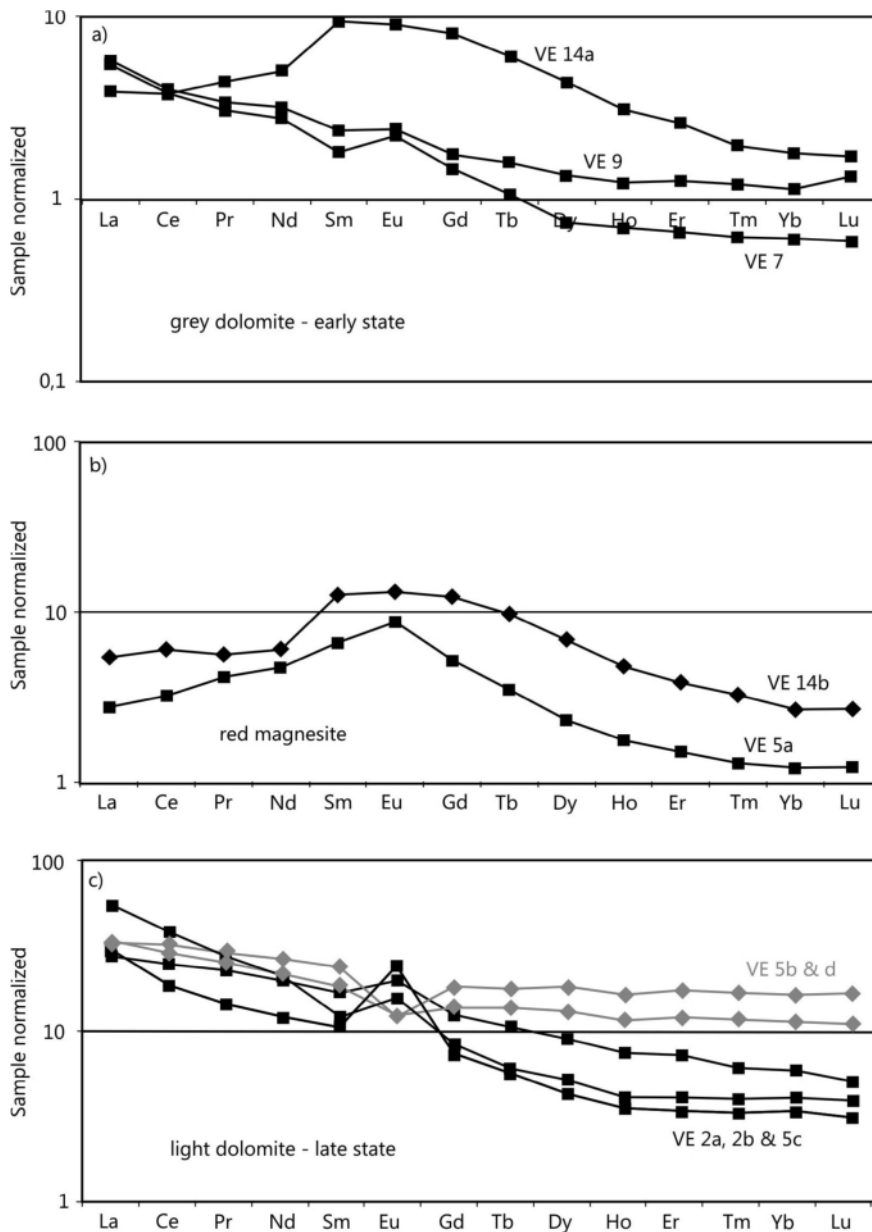


FIGURE 12: Chondrite-normalized REE patterns of different carbonate generations from the Veitsch magnesite deposit: a) residual grey dolomite, b) red magnesite, c) vein dolomite.

not deviate from typical samples as the ones analyzed in Deer et al. (1992) except for a higher content of FeO (0.98 – 3.00 wt%). However the early state magnesite samples have low Sr (32 – 77 ppm) and Y (1.2 – 5 ppm) contents - more similar to the respective contents in the magnesite samples.

In the Wald am Schober magnesite deposit the majority of the magnesite samples is characterized by the following elements: MgO (38.58 – 46.90 wt%), CaO (0.44 – 5.02 wt%), MnO (0.07 – 0.10 wt%). FeO is slightly elevated (1.23 – 2.20 wt%). SiO₂ contents are generally low (1.09 – 2.89 wt%) but elevated in certain magnesite samples (WS2, WS11, WS12, WS20) (4.94 – 14.05 wt%). A similar trend is detectable in the Sr content of certain samples. Most samples have expectably low Sr contents (2-6 ppm), but samples WS 9ca, WS9cb and WS 20 have significantly higher Sr contents (19-46 ppm). Other major, minor and trace elements do not show any significant variations or trends. Dolomite samples follow the general geochemical composition of dolomites with MgO (20.22 – 21.28 wt%), CaO (28.98 – 30.03 wt%), FeO (0.12 – 0.54 wt%) and MnO (0.02 – 0.04 wt%). Sr contents are between 65 ppm (WS1) and 116 and 119 (WS7 and WS8 respectively).

The samples taken outside the Las-

sing talc deposit are calcite marble with MgO (0.68 – 5.19 wt%), CaO (49.1 – 53.51 wt%), FeO (0.11 – 0.51 wt%) and MnO (0.01 – 0.08 wt%). The handspecimen from inside the deposit are dolomite with MgO (13.73 – 22.39 wt%), CaO (24.67 – 33.1 wt%), FeO (0.36 – 0.8 wt%) and Mn (0.02 – 0.07 wt%).

4.3 REE PATTERN

Ratios of La/Yb were calculated according to Goldstein and Jacobsen 1988 and are listed in table 1-3.

REE patterns of carbonates from the Veitsch magnesite deposit show certain distinct features according to their type and generation. The precursor grey dolomite (VE 9 and VE 7) shows a pattern of REE with lower values of HREE and a moderate positive Eu anomaly (Fig. 12a). Sample VE 14a is an exception with a roof-shaped REE pattern. The red magnesite of samples VE 14b and VE 5a shows a similar roof-shaped pattern with slightly lower HREE (Fig. 12b). The REE pattern of the younger vein dolomite can be differentiated from earlier carbonate generations of the Veitsch deposit. They show a general downward directed REE pattern with lower values of HREE but with a prominent positive (VE 2a, 2b, and 5c) and negative (VE 5b and d) Eu anomaly (Fig. 12c). REE contents of carbonates with contents of SiO₂ and Al₂O₃ show no positive correlation.

The magnesite samples from the Wald am Schober deposit show no significant distinction in their REE pattern. All samples (whether free of talc or with disperse talc accumulations) have a roof shaped REE pattern. Only two samples show a more prominent Eu anomaly (Fig. 13b). However samples in contact with the talc bearing shear zones have a very prominent negative Eu anomaly with a general roof shaped REE pattern. The late state "horse tooth dolomite" is very enriched in REE compared to other samples from the deposit with a roof shaped REE pattern. And the hostrock (dolomite marble) has a downward directed REE pattern with low HREE values (Fig. 13a).

The REE patterns at the Lassing talc deposit show a lot more variation in their respective groups than the samples at the other deposits. Calcitic marbles from outside the deposit are depleted in HREE and

have a downward REE trend with partly positive and negative Eu anomaly (Fig. 14a). A similar pattern can be observed from the dolomite marble inside the deposit with partly more pronounced negative and positive Eu anomalies (Fig. 14b). Eu anomalies can be an important indicator for temperature estimations and the origin of the mineralizing fluid (Bau, 1991).

4.4 STABLE ISOTOPES

Stable Isotopes of carbonates and quartz were analyzed at different locations within the Eastern Greywacke Zone (Tab. 4).

Carbon isotope values at the Veitsch magnesite deposit range from $\delta^{13}\text{C} = -7.00$ to -1.68‰ (VPDB) and oxygen isotope values range from $\delta^{18}\text{O} = 13.04$ to 20.16‰ (VSMOW, Fig. 15). The different genetic rock groups show distinct trends. The early state grey dolomite has lowest values of $\delta^{13}\text{C}$ and $\delta^{18}\text{O}$. Also the dolomite veins are depleted in $\delta^{18}\text{O}$ compared to magnesite samples. The magnesite samples from the deposit spread more but have a tendency to higher $\delta^{13}\text{C}$ and $\delta^{18}\text{O}$ val-

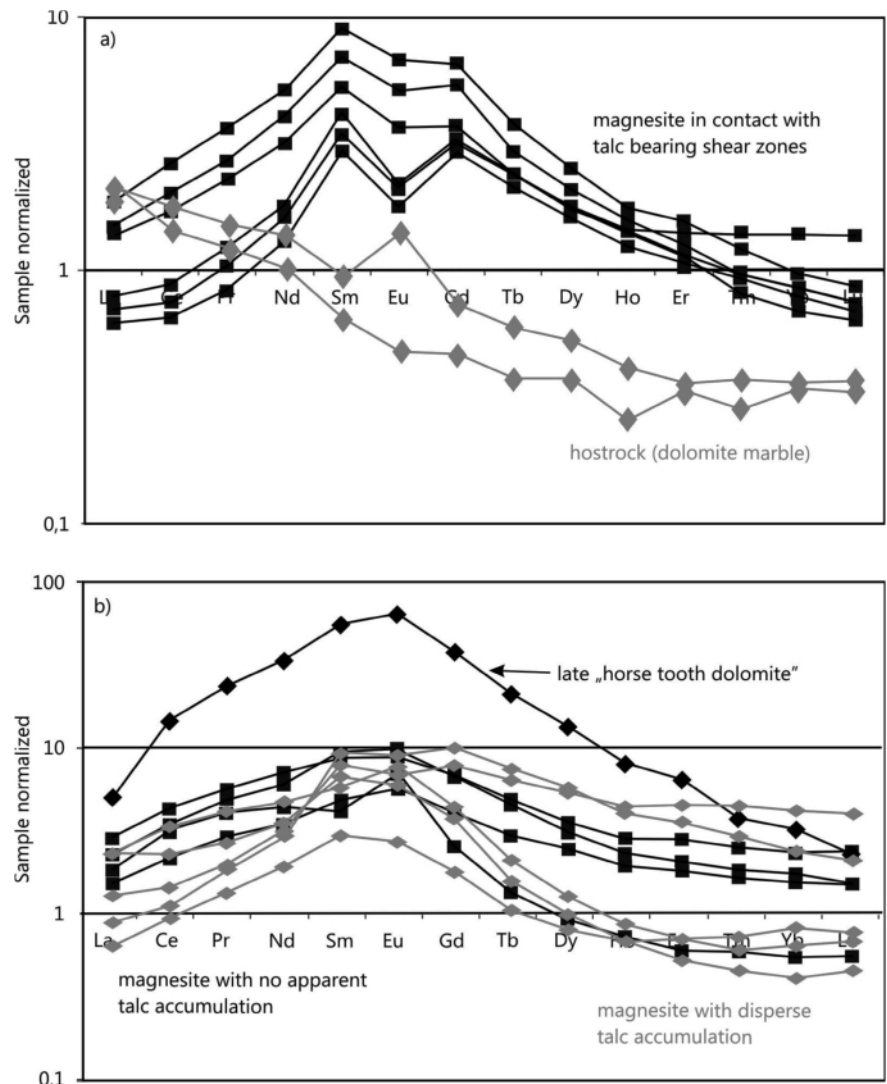


FIGURE 13: Chondrite-normalized REE patterns of different carbonate generations from the Wald am Schober magnesite deposit: a) magnesite in contact with talc bearing shear zones and hostrock dolomite marble b) magnesite with disperse talc accumulation and magnesite with no apparent talc accumulation, late state "horse tooth dolomite".

Sample	Mineral	$\delta^{18}\text{O}$ [VSMOW]	$\delta^{13}\text{C}$ [VPDB]	remarks
VE 1 a	dol	13.64	-1.68	vein
VE 1 b	mgs	15.82	-4.72	red
VE 1 c	dol	14.14	-2.38	vein
VE 1 d	mgs	15.82	-4.52	red
VE 1 e	mgs	15.53	-3.93	red
VE 2a a	mgs	19.98	-5.42	red
VE 2a b	dol	16.97	-5.83	vein
VE 2b a	mgs	15.55	-2.84	red
VE 2b b	mgs	20.16	-2.81	red
VE 2b c	dol	14.56	-2.26	vein
VE 2b d	dol	13.67	-2.21	vein
VE 2b e	dol	13.72	-3.09	vein
VE 4 a	dol	13.72	-1.93	vein
VE 4 b	mgs	17.97	-4.99	red
VE 5 a	mgs	13.30	-2.29	red
VE 5 b	dol	13.04	-2.02	vein
VE 5 c	dol	15.19	-3.11	vein
VE 5 d	dol	15.12	-3.32	vein
VE 6 a	mgs	16.92	-2.93	red
VE 6 b	dol	13.63	-2.12	vein
VE 6 c	dol	13.55	-1.84	vein
VE 6 e	dol	15.98	-2.12	vein
VE 6 f	dol	13.87	-2.01	vein
VE 6 g	mgs	15.81	-3.12	red
VE 7 a	dol	14.19	-5.30	grey, marble
VE 8 a	dol	13.46	-6.33	grey, marble
VE 8 b	dol	13.59	-6.80	grey, marble
VE 9 a	dol	14.41	-7.00	grey, marble
VE 10 a	dol	27.21	-3.59	coral
VE 10 b	dol	27.44	-3.37	coral
VE 14 a	dol	25.46	-5.29	grey, marble
VE 14 b	dol	28.22	-2.61	grey, marble
VE 14 c	mgs	26.74	-4.04	red
VE 14c	mgs	14.72	-4.40	red
VE 14a	dol	14.13	-5.55	grey, marble
VE 14b	dol	15.58	-4.89	grey, marble
VE 1 f	qtz	14.95		vein
VE 4 c	qtz	15.22		vein
VE 5 e	qtz	15.42		vein
VE 7 b	qtz	14.70		vein
VE 9 b	qtz	15.21		vein
LA 2 a	cc	26.64	4.20	marble
LA 3 a	cc	19.60	1.48	marble
LA 4 a	cc	16.67	0.41	marble
LA 8 a	cc	20.42	0.92	marble
LA 9 a	cc	14.13	-1.11	marble
LA 10 a	cc	14.10	-0.88	marble
LA 11 a	cc	15.40	0.68	vein
LA 12 a	cc	19.79	-0.02	marble
LA PR 48	dol	13.53	-1.12	marble
LA PR 33	mgs	15.40	-0.32	
LA PR 65	dol	13.66	-1.24	marble
LA PR 101	dol	15.92	0.72	marble
LA PR 85	dol	15.88	0.71	marble
LA PR 31	dol	15.72	1.57	marble
LA 1 b	qtz	16.20		vein
LA 4 b	qtz	17.84		vein
LA 5	qtz	16.56		vein
LA 6	qtz	16.84		vein
WS 1 a	dol	11.64	-2.98	vein
WS 3 a	mgs	12.86	-2.08	containing talc
WS 12 a	mgs	20.47	-12.88	containing talc
WS 2 a	mgs	12.18	-2.38	no talc
WS 4 a	mgs	12.44	-2.26	no talc
WS 9b a	mgs	12.89		close to shearzone
WS 9b b	mgs	12.87	-3.42	close to shearzone
WS 9c a	mgs	15.30	-2.95	close to shearzone
WS 9c b	mgs	15.03	-3.92	close to shearzone
WS 11 a	mgs	13.48	-3.08	containing talc
WS 20 a	mgs	12.92	-3.09	containing talc
WS 21 a	mgs	12.51	-3.11	containing talc
WS 10b a	mgs	12.22	-3.37	close to shearzone
WS 10b b	mgs	12.24	-3.38	close to shearzone
WS 23 a	mgs	12.78	-1.73	no talc
WS 23 b	mgs	12.82	-2.05	no talc
SU 1	cc marble	27.25	1.73	hostrock
SU 2	cc marble	28.47	2.05	hostrock
WS 7 a	dol marble	20.46	-0.17	hostrock
WS 8 a	dol marble	17.34	-1.13	hostrock

TABLE 4: Stable isotope data from locations within the Eastern Greywacke Zone

ues. Generally all carbonate samples are depleted in their $\delta^{13}\text{C}$ and $\delta^{18}\text{O}$ values compared to seawater.

Oxygen isotope values of quartz from veins are in the range of $\delta^{18}\text{O} = 14.7$ to 15.42‰ . (VSMOW).

At the Wald am Schober magnesite deposit carbon isotope values range from $\delta^{13}\text{C} = -3.92$ to -0.17‰ . (VPDB) and oxygen isotope values are in the range of $\delta^{18}\text{O} = 11.64$ to 20.46‰ . (VSMOW, Fig. 15). Magnesite samples have generally a tendency to lower $\delta^{18}\text{O}$ values compared to the magnesite samples from the Veitsch deposit. Distinction between the different magnesite groups are not as obvious as at the Veitsch deposit where magnesites show a much clearer distinction from the late state dolomite veins. The hostrock dolomite marble represents another group with a tendency to higher $\delta^{13}\text{C}$ and $\delta^{18}\text{O}$ values than the magnesite from the deposit.

Samples of dolomite from the Lassing talc deposit have carbon isotope values in the range of $\delta^{13}\text{C} = -1.24$ to 1.57‰ (VPDB) and oxygen isotope values in the range of $\delta^{18}\text{O} = 13.66$ to 20.42‰ (VSMOW, Fig. 15).

4.5 ION-CHROMATOGRAPHY

Fluid inclusions were analyzed using Ion-chromatography at different locations within the Eastern Greywacke Zone (Tab. 5).

At the Veitsch magnesite deposit fluid inclusions of magnesite, early and late state dolomite and secondary quartz were analysed (Fig. 16). All samples have low Na/Br (< 405) and Cl/Br (< 513) ratios compared to modern seawater. Samples from early state dolomite have especially low values (Na/Br < 78 and Cl/Br < 123). Li/Na ratios are also low (< 0.0135) with no apparent trend.

Na-K-temperatures for carbonates calculated according to Can (2002) are low at around 180°C . Na-K-temperatures are significantly higher at 340°C for secondary quartz.

Charge balance ($Q+/Q-=1$) for carbonates is imperfect with values between 4 and 5 but comes close to 1 for the quartz samples with around 1.4. The imperfect charge balance within the carbonate samples might be due to volatile phases lost during the crushing process.

At the Wald am Schober magnesite deposit samples are also generally lower than modern seawater (with Na/Br < 290 and Cl/Br < 350) and lower than samples from the Veitsch deposit (Fig. 16). Only samples VE7 and VE8 (hostrock from outside the deposit) come close to the values of modern seawater.

Na-K-temperatures (calculated according to Can, 2002) are at 248°C for magnesite from the deposit and at 184°C for samples VE7 and VE8.

Charge balance ($Q+/Q-=1$) for carbonates is also imperfect with values between 4 and 8.

The Lassing talc deposit shows low Na/Br and Cl/Br ratios for samples from inside the deposit (Na/Br < 440 and Cl/Br < 500). Samples from outside the deposit vary greatly from values below the values of modern seawater and values well beyond the values of modern seawater (Fig. 16).

Na-K-temperatures of carbonate samples from inside the deposit are at around 140°C . Temperatures of carbonate samples

from outside are higher with 200°C and quartz temperatures are even as high as 360°C.

Charge balance ($Q+/Q-=1$) for carbonates are again imperfect and vary for samples from outside the deposit between 2 and 3 and for samples from inside the deposit between 3 and 9. However quartz samples from outside are close to perfect charge balance with values between 1.2 and 1.4.

5. DISCUSSION

The deposits discussed in this paper are bound to the tectonic evolution of the Eastern Alps. The Veitsch magnesite deposit is about 7 km from the Mur- Mürz-Fault and at the nappe boundaries of Silberberg nappe and Veitsch nappe, the Wald am Schober magnesite deposit is in direct vicinity to the Palental-Liesingtal-Fault and the Lassing talc deposit is situated at the junction of the Palental-Liesingtal-Fault and the SEMP Palental-Liesingtal-Fault and the Lassing talc deposit is situated at the junction of the Palental-Liesingtal-Fault and the SEMP (Fig. 2) and also close to ductile nappe boundaries. The causes for talc mineralization within the magnesite bodies of the Veitsch nappe will be discussed.

5.1 VEITSCH DEPOSIT

The brittle structures of the Veitsch deposit propose that deformation took place under low temperature conditions. Field observations suggest several geological events: The greyish dolomite can be regarded as a precursor rock. It is consumed to a large extent by reddish coarsely grained sparry magnesite. Residuals of the precursor dolomite are present throughout the deposit. Partly, it can be seen that very distinct grains of magnesite have evolved from the dolomite. In other parts magnesitization has progressed further and only very small residuals of dolomite are left. Due to its low Na/Br and Cl/Br (typically Cl/Br = 658 according to Gleeson, 2003) ratios that indicate an evaporitic origin of the mineralizing fluid Prochaska (2000) explains the magnesite formation with residual evaporitic brines that percolated through the crust during Permoskythian rifting.

High heatflow during rifting (Schuster et al., 1999) induced hydrothermal convection systems and allowed highly evaporated seawater to percolate the crust and mineralize the dolomite rocks to magnesite. Tem-

peratures of fluid inclusion study of the non-steatitized magnesite is estimated to be at approx. 180°C. With increasing metamorphism the $\delta^{13}\text{C}$ and $\delta^{18}\text{O}$ change towards lighter values (Schroll, 2002) which can be attributed to equilibration of the carbonates with metamorphic fluids (Kralik et al., 1989 and Schroll, 2002) or due to rising hot basinal brines of connate origin (Aharon, 1988). Precursor dolomite from the Veitsch deposit differs significantly in their $\delta^{13}\text{C}$ values from late state dolomite veins and magnesite. This can indicate the occurrence of multiple hydrothermal events or different precipitation mechanisms within the hydrothermal system (Hurai et al., 2011).

The REE pattern of the dolomitic precursor rock and the magnesite are similar in their general trend and their amount of REE. The characteristics of REE patterns are controlled by the composition of the migrating fluid, the mineralogical features of the hostrock and the physico-chemical conditions during precipitation (Bau and Möller, 1992). According to Möller (1989) the REE concentrations of purely marine magnesites are very low and become considerably higher if magnesite for-

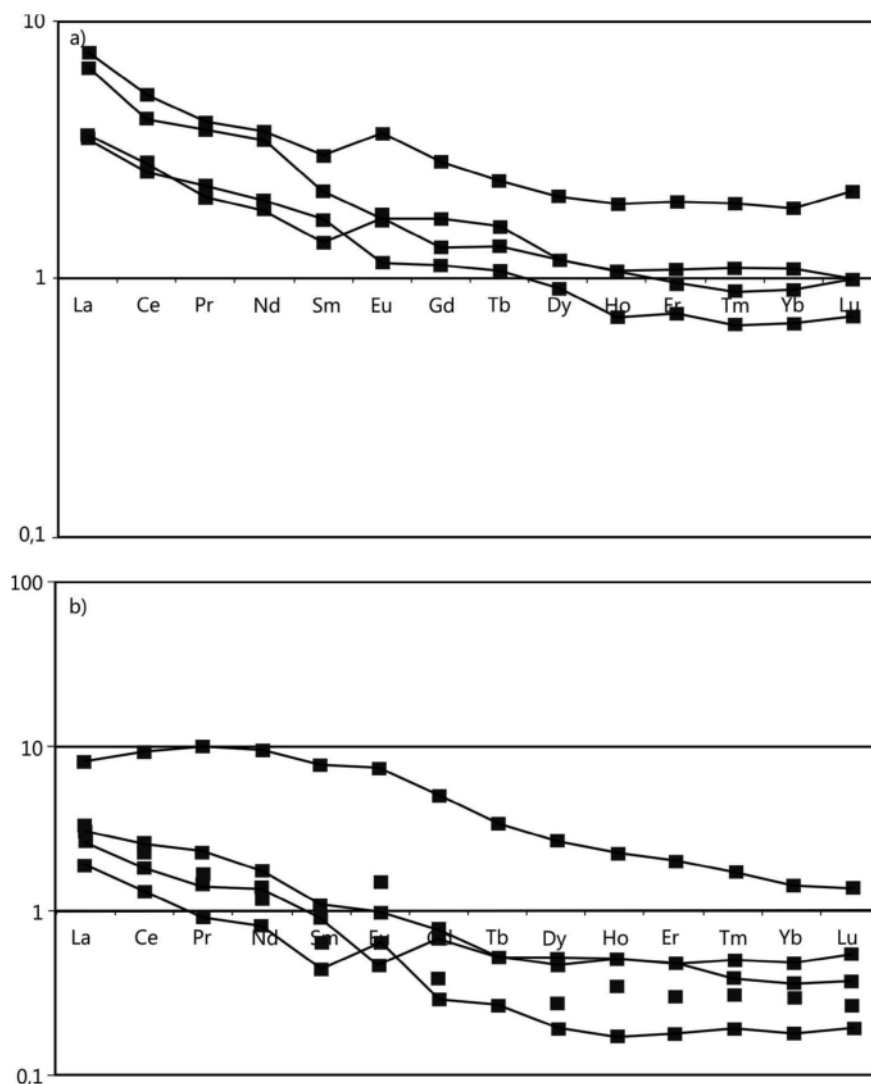


FIGURE 14: Chondrite-normalized REE patterns of different carbonate generations from the Lassing talc deposit: a) Calcitic marble from outside the deposit, b) dolomite marble from inside the deposit.

Sample unit	Mineral	Li ppb	Na ppb	K ppb	Mg ppb	Ca ppb	F ppb	Cl ppb	Br ppb	J ppb	NO ₃ 3\$ ppb	SO ₄ 4\$ ppb	Na/Br mol/mol	Cl/Br mol/mol
Lassing														
LA2	cc	8.54	14739.79	647.44	4047.86	8911.67	3.27	29663.19	25.57	7.79	398.93	708.71	2003.66	2615.01
LA4ges	cc	10.68	6621.17	606.65	4257.42	10174.54	2.66	17055.83	44.53	10.55	2061.85	422.96	516.81	863.37
LA1a	dol	5.17	3260.38	355.99	18405.80	5639.04	8.17	7524.68	27.70	4.84	283.00	288.35	409.05	612.24
LA1b	qtz	0.41	10745.65	1887.42	3172.13	1990.26	0.60	21258.79	68.93	6.50	n.a.	51.83	541.82	695.16
LA3	cc	0.20	4613.56	439.73	3786.83	7215.85	2.99	8557.84	14.25	8.32	n.a.	227.54	1125.18	1353.55
LA4a	qtz	0.40	10992.88	4019.72	2112.60	6401.80	1.59	25509.78	81.97	7.86	6.71	52.95	466.09	701.44
LA4b	cc	2.63	10113.99	897.71	3479.64	11842.07	2.24	18944.35	47.62	8.61	n.a.	424.01	738.12	896.62
LA5	qtz	0.17	5394.76	1798.79	363.55	2031.57	6.04	11389.06	60.61	5.07	1.98	50.21	309.33	423.50
LA6	qtz	0.09	6451.89	1673.02	361.08	2191.82	32.21	12428.38	63.40	4.71	1731.78	40.95	353.67	441.83
LA8	cc	0.93	7344.56	478.88	1224.84	9672.72	2.01	13831.75	20.90	6.46	n.a.	164.33	1221.33	1491.65
LA11a	cc	0.17	6734.21	414.97	892.50	18666.55	23.86	13773.09	21.56	8.13	n.a.	434.95	1085.60	1439.92
LA12	cc	1.22	6850.04	314.79	1618.18	11146.42	3.26	13177.18	15.77	4.66	n.a.	168.23	1509.38	1883.01
LA9a	cc	1.40	5678.90	302.90	4125.68	9998.67	14.67	11771.86	17.95	7.02	n.a.	1266.78	1099.64	1478.28
LA9b	cc	2.75	7842.61	406.40	3452.86	12272.10	11.50	18269.18	26.34	8.13	222.88	1355.31	1034.63	1563.03
LAPR31	dol	12.09	4046.19	205.85	24752.35	11456.63	4.31	6994.40	59.14	8.12	n.a.	280.35	237.78	266.57
LAPR33	mgs	16.64	4612.47	118.68	24531.44	8903.59	259.34	8700.17	89.15	6.54	n.a.	412.60	179.82	219.96
LAPR48	dol	5.96	4476.76	187.98	24685.60	3575.84	5.79	8928.66	136.93	6.08	n.a.	164.67	113.62	146.97
LAPR65	dol	3.38	3096.45	73.20	31742.08	9305.00	27.38	5468.88	24.35	6.43	n.a.	799.75	441.91	506.17
LAPR85	dol	16.62	4794.93	135.22	22738.07	8007.96	3.25	9103.74	96.63	9.60	n.a.	290.21	172.46	212.35
LAPR121	dol	1.14	3857.82	46.29	12150.07	5687.78	276.28	6963.30	14.00	6.19	n.a.	203.58	957.97	1121.37
Veitsch														
VE2a	mgs	1.80	2945.78	183.45	21002.06	7022.65	12.17	4884.30	50.63	2.66	n.a.	505.66	202.20	217.43
VE7a	dol	27.61	13898.30	740.64	25408.13	9203.67	1.25	24925.40	1191.27	3.64	n.a.	217.25	40.55	47.16
VE9a	dol	28.25	10606.67	529.47	25034.25	9715.04	1.76	21263.02	816.25	3.42	n.a.	321.07	45.16	58.71
VE14a	dol	25.63	6269.13	277.34	22689.40	9795.73	4.92	15982.99	433.98	3.32	n.a.	496.79	50.20	83.01
VE14c	mgs	3.78	3707.35	160.04	20349.72	7198.21	10.20	8570.55	195.68	3.86	n.a.	840.15	65.84	98.72
VE2b	dol	6.66	7789.85	336.38	21428.72	8950.31	4.47	13983.72	84.24	6.72	n.a.	214.47	321.36	374.12
VE5c	mgs	15.73	7480.36	302.21	18100.02	8966.82	0.63	13545.93	114.75	6.95	n.a.	156.41	226.56	266.07
VE5b	dol	15.53	12610.44	511.11	26263.21	10538.32	1.27	24613.28	108.01	7.62	n.a.	348.52	405.76	513.61
VE5d	mgs	17.96	10677.42	461.00	22915.38	10160.86	1.05	19813.15	133.14	7.84	n.a.	261.37	278.72	335.42
VE5a	mgs	1.60	5044.57	223.99	20179.85	4054.56	6.33	12128.75	222.00	4.63	208.04	232.55	78.97	123.14
VE1f	qtz	0.25	3942.43	744.60	4540.35	2473.61	0.93	7078.67	121.93	10.22	n.a.	60.50	112.37	130.85
VE5e	qtz	0.67	7261.25	2871.61	2822.29	1964.09	10.85	15952.18	88.97	6.59	n.a.	125.92	283.64	404.11
VE7b	qtz	5.46	13645.28	3149.88	1390.53	5959.00	3.01	27156.88	157.08	6.07	n.a.	124.96	301.90	389.65
VE9b	qtz	0.49	2364.39	456.49	356.46	1730.80	13.02	3066.82	29.69	2.34	704.00	72.33	276.80	232.84
VE4c	qtz	2.22	7407.45	1800.56	670.74	2317.39	7.39	14737.94	142.18	4.36	n.a.	209.62	181.07	233.64
Wald a. S.														
WS12	mgs	4.17	7986.24	790.60	23734.89	6074.61	4.86	17161.82	226.34	6.55	n.a.	128.69	122.63	170.90
WS9ca	mgs	4.63	6962.52	748.98	29605.79	6236.83	4.51	13648.45	99.66	8.97	n.a.	131.11	242.81	308.68
WS9cb	mgs	1.63	4552.28	516.72	20566.48	3890.85	5.50	8523.27	54.68	5.69	409.52	106.95	289.32	351.30
WS10ba	mgs	3.42	7485.18	762.17	21538.94	2033.60	6.91	18353.29	304.59	4.28	129.02	82.21	85.41	135.81
WS1	dol	32.88	8915.76	1205.18	20471.52	8892.07	1.09	19579.25	337.12	6.49	n.a.	76.41	91.91	130.90
WS2	mgs	6.48	8760.58	832.88	26573.17	3199.42	5.79	29283.39	735.82	5.83	49.24	84.33	41.38	89.70
WS3	mgs	19.43	11189.30	1490.48	28713.58	2831.39	6.64	29178.69	649.04	5.38	n.a.	81.27	59.92	101.33
WS4	mgs	4.34	9069.90	948.38	23312.01	1824.52	3.55	24165.24	544.94	6.33	n.a.	133.54	57.84	99.95
WS9bg	mgs	0.85	5139.45	598.76	20561.92	5514.44	44.46	10037.16	94.13	6.87	n.a.	67.53	189.75	240.32
WS11	mgs	1.99	6320.77	749.24	21321.58	2181.09	6.60	12983.49	213.01	6.29	n.a.	64.44	103.13	137.38
WS20	mgs	6.43	5992.93	605.11	23062.06	5178.61	16.43	12176.37	183.33	6.10	n.a.	97.61	113.61	149.70
WS21	mgs	2.75	8548.37	817.55	24278.88	1949.71	5.82	21440.38	380.66	6.41	166.30	78.10	78.05	126.95
WS23d	mgs	12.82	8379.18	1009.63	21435.26	1176.13	4.23	16961.15	341.17	5.50	n.a.	83.74	85.36	112.05
WS23h	mgs	7.40	7908.30	970.01	22608.17	1454.47	3.22	16383.65	321.03	5.64	111.13	110.80	85.61	115.02
hostrocks														
SU 1	cc	1.70	3048.42	522.28	4126.79	8965.10	259.19	5399.78	14.47	73.77	n.a.	6177.31	732.06	840.94
SU 2	cc	2.98	3177.33	110.28	2269.54	9368.84	63.55	5666.94	11.58	10.59	n.a.	440.84	953.51	1102.90
WS 7	dol	0.33	1419.72	87.98	20702.93	7471.85	4.71	1773.80	7.90	3.84	n.a.	89.67	624.93	506.36
WS 8	dol	1.44	2589.64	125.39	22451.13	8309.67	7.80	4872.30	15.24	4.49	n.a.	206.25	590.53	720.54

TABLE 5: Ion-chromatography data of fluid inclusions from locations within the Eastern Greywacke Zone

mation is caused by hydrothermal fluids during diagenesis. The similarity of the REE pattern of the magnesite and the dolomitic host rock reflects the genetic link between both rocks indicating that the magnesites formation can be attributed to Mg^{2+} metasomatism of the hostrock. The late-stage dolomite of the Veitsch deposit is depleted in HREE compared to LREE. This is a hint for remobilised fluids (Schroll, 1997) that led to the precipitation of the late stage dolomite. The varying positive and negative Eu anomaly supports that. The redox potential of Eu strongly depends on temperature, slightly on pH and is almost unaffected by pressure (Bau, 1991). At temperatures above 200°C Eu^{2+} dominates over Eu^{3+} and a positive Eu anomaly is formed (Bau and Möller, 1992).

Field evidences and analytical study from Veitsch support the model of Koch (1893) and Redlich (1909) of the epigenetic nature of magnesite formation.

Carbonate samples that represent the non-steatitized country rock "Triebensteinkalk" of the Sunk Formation (carbonate samples from outside the Lassing deposit, SU1, SU2, WS7, WS8) plot above the seawater ratio along the (halite-dissolution trend). However quartz samples of veins within the Triebensteinkalk country rock have lower Na/Br and Cl/Br ratios as seawater indicating a relation of the fluids from within the deposit and the quartz veins.

Na/K temperatures of the "Triebensteinkalk" country rock are equally low as temperatures from the Veitsch deposit. Also clearly higher $\delta^{18}O$ and $\delta^{13}C$ values are closer to that of marine carbonates.

5.2 WALD AM SCHOBERPASS

At the magnesite deposit Wald am Schober talc occurs as impurities within the carbonate hostrock body. The deposit is clearly marked by ductile deformation indicating higher temperature conditions. Precursor rocks were not found within the boun-

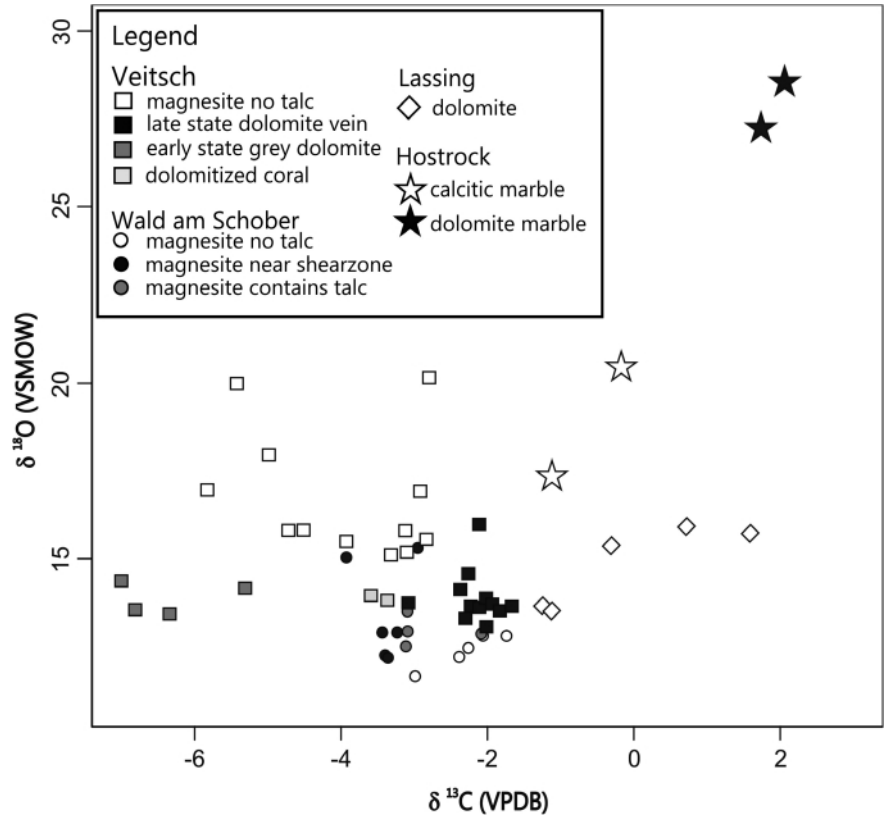


FIGURE 15: Stable Isotope data from Veitsch, Wald am Schober, Lassing and hostrocks.

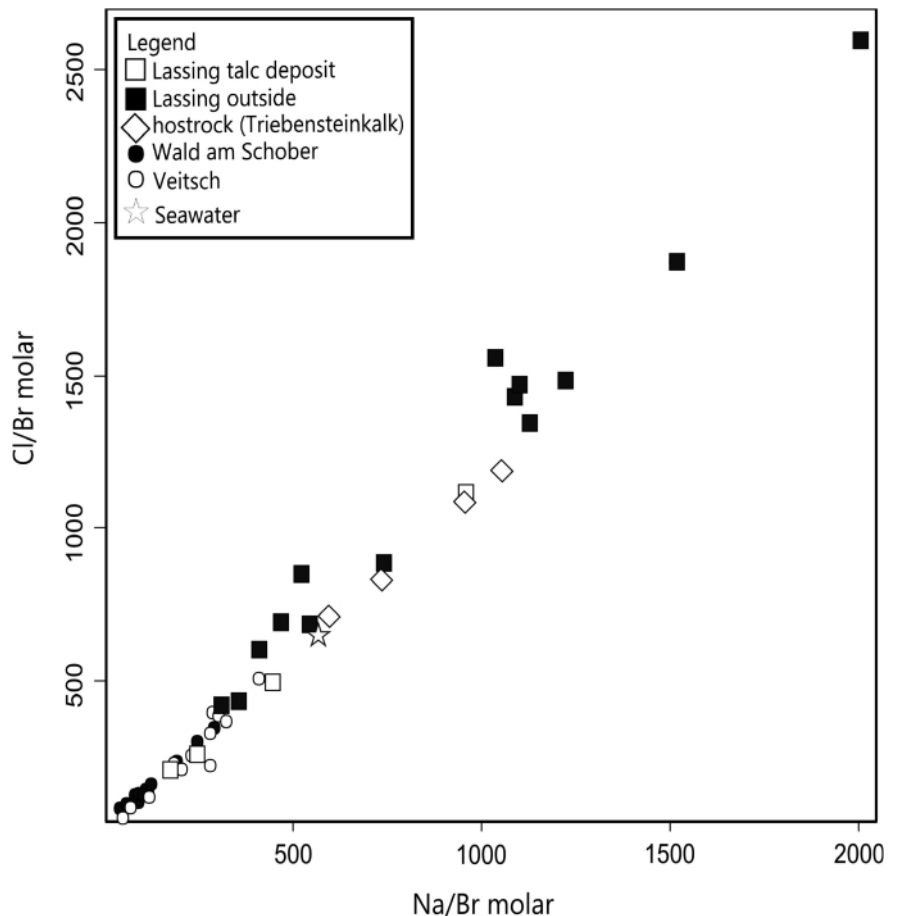


FIGURE 16: Crush leach data of deposits from the Eastern Greywacke Zone (Veitsch, Wald am Schober, Lassing and hostrock).

daries of the deposit. It can be assumed that the magnesite formed under similar conditions during Permoskythian rifting as the magnesite body at the Veitsch deposit. The coarsely grained greyish to whitish magnesite body is penetrated by shear zones. The fault core is composed of talc and a fine grained hyaline matrix of gouge material. Towards the magnesite hostrock fragments of carbonate rocks occur in a fine grained matrix. This indicates a decrease of deformation intensity from the fault core towards the magnesite hostrock. The talc shear zones are dominantly normal faults. The circulation of a silica-rich fluid through these shear zones may lead to dissolution of the magnesite hostrock and the precipitation of talc. The talc formation may have started to develop along fractures or as isolated patches within the hostrock and form interconnected networks as strain increases (Collettini et al., 2009). Na/Br and Cl/Br values of the carbonate rocks are again well below the corresponding ratios of seawater (typically Cl/Br = 658 according to Gleeson, 2003). Na-K temperatures of fluid inclusions however are significantly higher (approx. 250°C) than at the Veitsch deposit. Also lighter $\delta^{18}\text{O}$ values from the Wald am Schober deposit compared to values from the Veitsch deposit indicate higher fluid temperatures that penetrated the magnesite hostrock. The group of magnesite samples close to talc shear zones with lighter $\delta^{13}\text{C}$ may indicate an increase of temperature towards the shear zones. The magnesite samples also show the roof-shaped pattern very similar to the magnesites from the Veitsch deposit also indicating the formation of the magnesite by metamorphogenic hydrothermal fluids (Bau and Möller, 1992). However magnesite samples in close contact with the talc bearing shear zones at Wald am Schober have a very pronounced negative Eu anomaly.

Tectonic events may have induced enough stress to dissolve Mg from the magnesite hostrocks and to enrich talc in the existing fractures through circulating SiO₂-rich fluids. Ductile structures of Wald am Schober clearly postdate the magnesite formation. Also the higher temperatures compared to magnesite samples from Veitsch and the "Triebensteinkalk" country rock indicate that after magnesite formation a hydrothermal event took place that led to the formation of the talc within shear zones. According to Willingshofer et al. (1999a), Willingshofer et al. (1999b), Kurz and Fritz (2003) and Rantitsch et al. (2005) subsidence after Eoalpine orogeny that created the Gosau basins yielded tectonic structures and temperatures that are in agreement with the features at Wald am Schober. In that case nappe boundaries may have acted as fluid circuits and transport SiO₂-rich fluids. The east directed normal faults observed at Wald am Schober (Figure 8 a, b) can be interpreted as a result of the overall observed Late Cretaceous extension in the Eastern Alps (Ratschbacher 1986, Wagreich, 1995, Froitzheim et al., 1994, Neubauer et al., 1995, 2000).

The position of the Wald am Schober deposit at the Paltental-Liesingtal-Fault also need some consideration. However not much is known about the Paltental-Liesingtal-Fault except

for its dextral sense of shear (Linzer et al., 2002), its position within the Miocene escape tectonic fault system of the eastern Alps and its brittle nature (Brosch and Kurz, 2008). These arguments of temperature and deformation structures may outrule a possible link of the talc shear zones at Wald am Schober and the Miocene Paltental-Liesingtal-Fault.

5.3 LASSING DEPOSIT

The carbonates surrounding the Lassing talc mine show multiple deformational events as well as a post tectonic phase. The talc mine is situated at the junction of two fault zones (Paltental-Liesingtal-Fault and SEMP). Structural data from the Lassing talc mine from Neubauer (2001) confirms the multiphase deformation phases and reveals some insights on the geology of the mine: Talc forms lenses and bodies confined by anastomosing fault planes. Lenses of talc represent the fault core while hostrocks constitute shear lenses or even boudins. The structures are related to NNE-SSW shortening and subvertical extension. The formation of such large talc bodies can be related to the activity of the fault zone with hot Si-bearing fluids concentrated within shear zones that formed networks of shear zones dissolving Mg from the hostrock. After all Mg was used and abundant Si reactant was left over veins of quartz formed. Quartz samples from Lassing have high Na-K temperatures (340°C). The large formation of talc was possible due to a rich occurrence of Mg carbonates and large amounts of Si bearing fluids.

However such bodies are not seen in the Wald am Schober deposit which is also related to the Paltental-Liesingtal-Fault. Jordan (1987) and Handy (1990) describe experiments and modelling that show the importance of rheology difference of materials for the formation of such bodies. The weak mineral phase becomes enriched and more abundant with increasing strain in fault cores and forms large bodies while the stronger mineral phase remains in internally less deformed shear lenses.

The Na/Br and Cl/Br ratios from Lassing are as well below the ratio of seawater and plot along the seawater evaporation line. Na/K temperatures are approx. 140-200°C.

The carbonate samples from the Lassing talc deposit have a tendency to reflect the signature of marine carbonates with $\delta^{13}\text{C}$ values around 0. The reason can be found in the impermeability of marbles during metamorphism (Nabelek et al., 1984). As a barrier they impede fluid flow and thus homogenization with the metamorphic fluid and keep their original sedimentary isotopic signature (Valley et al., 1990).

The carbonates from the Lassing deposit do not show a clear roof shaped REE pattern as the carbonates from Veitsch and Wald am Schober. The Lassing samples have a tendency of depleted HREE and enrichment of LREE.

5.4 CONCLUSION

The study shows the significance of fault zones to the formation of talc. Even though talc mineralization is not exclusively linked to fault zone (Evans and Guggenheim, 1991), it did play an important role for its formation in the eastern Grey-

wacke zone. The deposits investigated in this study are of similar hostrocks but differ in their distance to the fault zone. The Veitsch deposit is furthest away from the Mur-Mürz-Fault and no talc occurrence is reported. In addition geochemical analysis and field study supports the low deformation and low temperature metamorphism at the deposit. For the Wald am Schober deposit at the Paltental-Liesingtal-Fault higher deformation and temperature are reported and talc occurs as impurities along discrete cm to dm thick shear zones. Deformation structures and temperatures may be linked to subsidence events following Eo-alpine orogeny. The Lassing talc deposit was - until its closure in 1998 - the second largest talc mine in Austria. Its tectonic features give hints of high deformation along one of the major Oligocene to Miocene fault zones of the Eastern Alps.

ACKNOWLEDGMENTS

The study was funded by UZAG (Universitätszentrum für Angewandte Geowissenschaften at the University of Leoben). The authors gratefully acknowledge the constructive review of Franz Neubauer and Petr Jeřábek as well as the careful editorial treatment by Ralf Schuster.

REFERENCES

- Aharon, P., 1988. A stable-isotope study of magnesites from the Rum Jungle uranium field, Australia: implications for the origin of strata-bound massive magnesites. *Chemical Geology*, 69, 127-145. [http://dx.doi.org/10.1016/0009-2541\(88\)90164-7](http://dx.doi.org/10.1016/0009-2541(88)90164-7)
- Bau, M., 1991. Rare-Earth element mobility during hydrothermal and metamorphic fluid-rock interaction and the significance of the oxidation state of europium. *Chemical Geology*, 93, 219-230. [http://dx.doi.org/10.1016/0009-2541\(91\)90115-8](http://dx.doi.org/10.1016/0009-2541(91)90115-8)
- Bau, M. and Möller, P., 1992. Rare Earth Element Fractionation in Metamorphogenic Hydrothermal Calcite, Magnesite and Siderite. *Mineralogy and Petrology*, 45, 231-246. <http://dx.doi.org/10.1007/BF01163114>
- Bottrell, S., Yardley, B. and Buckley, F., 1988. A modified crush-leach method for the analysis of fluid inclusion electrolytes. *Bulletin de Mineralogie*, 111, 297-290.
- Boulvais, P., de Paseval, P., D'Hulst, A. and Paris P., 2006. Carbonate alteration associated with talc-chlorite mineralization in the eastern Pyrenees, with emphasis on the St. Barthelemy Massif. *Contributions to Mineralogy and Petrology*, 88, 499-526. <http://dx.doi.org/10.1007/s00710-006-0124-x>
- Brosch, F. and Kurz, W., 2008. Fault damage zone dominated by high-angle fractures within layer-parallel brittle shear zones: examples from the eastern Alps. In: C. Wibberley, W. Kurz, J. Imber, R. Holdsworth and C. Collettini (eds.), *The internal Structure of Fault Zones: Implications for Mechanical and Fluid-Flow Properties*. Geological Society London, Special Publications, 299, pp. 75-95.
- Can, I., 2002. A new improved Na/K geothermometer by artificial neural networks. *Geothermics*, 31, 751-760. [http://dx.doi.org/10.1016/S0375-6505\(02\)00044-5](http://dx.doi.org/10.1016/S0375-6505(02)00044-5)
- Caporali, A., Neubauer, F., Ostini, L., Stangl, G. and Zuliani, D., 2013. Modeling surface GPS velocities in the Southern and Eastern Alps by finite dislocations at crustal depths. *Tectonophysics*, 590, 136-150. <http://dx.doi.org/10.1016/j.tecto.2013.01.016>
- Collettini, C., Viti, C., Smith, S. and Holdsworth, R., 2009. Development of interconnected talc networks and weakening of continental low-angle normal faults. *Geology*, 37, 567-570. <http://dx.doi.org/10.1130/G25645A.1>
- Collombet, M., Thomas, J.-C., Chauvin, A., Tricart, P., Bouillin, J.-P. and Gratier, J.-P., 2002. Counterclockwise rotation of the Western Alps since the Oligocene: new insights from paleomagnetic data. *Tectonics*, 21, 14-21. <http://dx.doi.org/10.1029/2001TC901016>
- Decker, K. and Peresson, H., 1996. Tertiary kinematics in the Alpine – Carpathian – Pannonian system: Links between thrusting, transform faulting and crustal extension. In: G. Wessely and W. Liebl, (eds.), *Oil and Gas in Alpidic Thrustbelts and Basins of Central and Eastern Europe*. EAGE Special Publication, 5, 69-77.
- Deer, W., Howie, R. and Zussman, J., 1992. *An Introduction to the Rock Forming Minerals*. Pearson Education Limited, p. 498.
- Evans, B. and Guggenheim, W., 1991. Talc, pyrophyllite, and related minerals. In: S. Bailey (ed.), *Hydrous Phyllosilicates (exclusive of micas) - Reviews in Mineralogy*. Mineralogical Society of America, 19, pp. 225-294.
- Felser, K., 1977. Die stratigraphische Stellung der Magnesitvorkommen in der östlichen Grauwackenzone (Steiermark, Österreich). *BHM*, 122(2a), 17-23.
- Frisch, W., Kuhlemann, J., Dunkel, I. and Brügel, A., 1998. Palinspastic reconstruction and topographic evolution of the Eastern Alps during late Tertiary tectonic extrusion. *Tectonophysics*, 297, 1-15. [http://dx.doi.org/10.1016/S0040-1951\(98\)00160-7](http://dx.doi.org/10.1016/S0040-1951(98)00160-7)
- Froitzheim, N., Schmid, S.M., and Conti, P., 1994. Repeated change from crustal shortening to orogen-parallel extension in the Austroalpine units of Graubünden, *Eclogae Geologicae Helvetiae*, 87, 559-612.
- Genser, J. and Neubauer, F., 1989. Low angle normal faults at the eastern margin of the Tauern Window (Eastern Alps). *Mitteilungen der Österreichischen Geologischen Gesellschaft*, 81, 233-243.
- Gleeson, S. 2003. Bulk analysis of electrolytes in fluid inclusions. In: Samson, I., Anderson, A. and Marshall, D. (eds.), *Fluid inclusions: analysis and interpretation*. Mineralogical Association of Canada, 32, pp. 233-246.

- Goldstein, S.J. and Jacobsen, S.B., 1988. Rare earth elements in river water. *Earth and Planetary Science Letters*, 89, 35-47. [http://dx.doi.org/10.1016/0012-821X\(88\)90031-3](http://dx.doi.org/10.1016/0012-821X(88)90031-3)
- Handler, R., Dallmeyer, R.D., D. and Neubauer, F., 1997. $^{40}\text{Ar}/^{39}\text{Ar}$ ages of detrital white mica from Upper Austroalpine units in the Eastern Alps, Austria: Evidence for Cadomian and contrasting Variscan sources. *Geologische Rundschau*, 86, 69- 80.
- Handy, M., 1990. The Solid-State Flow of Polymineralic Rocks. *Journal of Geophysical Research*, 95, 8647-8661. <http://dx.doi.org/10.1029/JB095iB06p08647>
- Hurai, V., Huraiová, M., Koděra, P., Prochaska, W., Vozárová, A. and Dianiška, I., 2011. Fluid inclusion and stable C-O isotope constraints on the origin of metasomatic magnesite deposits of the Western Carpathians, Slovakia. *Russian Geology and Geophysics*, 52, 1474-1490. <http://dx.doi.org/10.1016/j.rgg.2011.10.015>
- Jordan, P., 1987. The deformational behaviour of bimineralic limestone – halite aggregates. *Tectonophysics*, 135, 185-197. [http://dx.doi.org/10.1016/0040-1951\(87\)90160-0](http://dx.doi.org/10.1016/0040-1951(87)90160-0)
- Kasemann, S., Meixner, A., Rocholl, A., Vennemann, T., Schmitt, A. and Wiedenbeck, M., 2001. Boron and oxygen isotope composition of certified reference materials NIST SRM 610/612, and reference materials JB-2G and JR-2G. *Geostandard Newsletter*, 25, 405-416. <http://dx.doi.org/10.1111/j.1751-908X.2001.tb00615.x>
- Koch, M., 1893. Mitteilung über einen Fundpunkt von Untercarbon-Fauna in der Grauwackenzone der Nordalpen. *Zeitschrift der Deutschen Geologischen Gesellschaft*, 45, 198-294.
- Kralik, M., Aharon, P., Schroll, E. and Zachmann, D., 1989. Carbon and oxygen isotope systematics of magnesites. In: Möller, P. (Ed.), *Magnesite – Geology, Mineralogy, Geochemistry, Formation of Mg-Carbonates*. Gebrüder Borntraeger Monograph Series on Mineral Deposits, 28, pp. 197-223.
- Kurz, W. and Fritz, H., 2003. Tectonometamorphic Evolution of the Austroalpine Nappe Complex in the Central Eastern Alps – Consequences for the Eo-Alpine Evolution of the Eastern Alps. *International Geology Review*, 45, 1100-1127. <http://dx.doi.org/10.2747/0020-6814.45.12.1100>
- Linzer, H.G., Moser, F., Nemes, L., Ratschbacher, L. and Sperner, B., 1997. Build-up and dismembering of the eastern Northern Calcareous Alps. *Tectonophysics*, 272, 97-124. [http://dx.doi.org/10.1016/S0040-1951\(96\)00254-5](http://dx.doi.org/10.1016/S0040-1951(96)00254-5)
- Linzer, H.G., Decker, K., Peresson, H., Dell'Mour, R. and Frisch, W., 2002. Balancing lateral orogenic float of the Eastern Alps. *Tectonophysics*, 354, 211-237. [http://dx.doi.org/10.1016/S0040-1951\(02\)00337-2](http://dx.doi.org/10.1016/S0040-1951(02)00337-2)
- Moine, B., Fortuné, J., Moreau, P. and Viguier, F., 1989. Comparative mineralogy, geochemistry, and conditions of formation of two metasomatic talc and chlorite deposits: Trimouns (Pyrenees, France) and Rabenwald Eastern Alps, Austria. *Economic Geology*, 84, 1398-1416. <http://dx.doi.org/10.2113/gsecongeo.84.5.1398>
- Möller, P., 1989. Minor and trace elements in magnesite. In: Möller, P. (Ed.), *Magnesite – Geology, Mineralogy, Geochemistry, Formation of Mg- Carbonates*. Gebrüder Borntraeger Monograph Series on Mineral Deposits, 28, pp. 173-195.
- Nabelek, P., Labotka, T., O'Neil, J. and Papike, J., 1984. Contrasting fluid/rock interaction between the Notch Peak granitic intrusion and argillites and limestones in western Utah: evidence from stable isotopes and phase assemblages. *Contributions to Mineralogy and Petrology*, 86, 25-43. <http://dx.doi.org/10.1007/BF00373708>
- Neubauer, F., Handler, R., Hermann, S. and Paulus, G., 1993. Tectonostratigraphy and structure of the east Graywacke Zone, Eastern Alps. *Mitteilungen der Österreichischen Geologischen Gesellschaft*, 87, 61-74.
- Neubauer, F., Handler, R., Hermann, S. and Paulus, G., 1994. Revised Lithostratigraphy and Structure of the Eastern Graywacke Zone (Eastern Alps). *Mitteilungen der Österreichischen Geologischen Gesellschaft*, 86, 61- 74.
- Neubauer, F., Dallmeyer, R.D., Dunkl, I. and Schirnik, D., 1995. Late Cretaceous exhumation of the metamorphic Gleinalm dome, Eastern Alps: Kinematics, cooling history and sedimentary response in a sinistral response corridor. *Tectonophysics*, 242, 79-98. [http://dx.doi.org/10.1016/0040-1951\(94\)00154-2](http://dx.doi.org/10.1016/0040-1951(94)00154-2)
- Neubauer F., Hoinkes, G., Sassi, F.P., Handler, R., Höck, V. and Koller, F., 2000. Pre-Alpine metamorphism of the Eastern Alps. *Schweizer Mineralogische und Petrographische Mitteilungen*, 79, 41–62.
- Neubauer, F., 2001. Structural control on the formation of talc deposits: Lassing, Austria. In: Piestrzynski, A. (ed.), *Mineral Deposits at the Beginning of the 21st Century*. Swets and Zeitlinger Publishers Lisse, pp. 1011-1014.
- Neubauer, F., Frisch, W. and Hansen, B.T., 2002. Early Palaeozoic tectonothermal events in basement complexes of the eastern Greywacke Zone (Eastern Alps): evidence from U-Pb zircon dating. *International Journal of Earth Science*, 91, 775-786. <http://dx.doi.org/10.1007/s00531-001-0254-7>
- Plan, L., Grasemann, B., Spötl, C., Decker, K., Boch, R. and Kramers, J., 2010. Neotectonic extrusion of the early Alps: Constraints from U/Th dating of tectonically damaged speleothems. *Geology*, 38, 483-486. <http://dx.doi.org/10.1130/G30854.1>

- Polgári, M., Prochaska, W. and Beran, A., 2010. Alpine carbonate mining sites: Aspects of carbonate mineralizations related to the manganese mine of Úrkút, Hungary, the magnesite deposit of Veitsch and the siderite mine Steirischer Erzberg, Austria. *Acta Mineralogica-Petrographica*, 4, 1-16.
- Prochaska, W., 1989. Geochemistry and genesis of Austrian talc deposits. *Applied Geochemistry*, 4, 511-525. [http://dx.doi.org/10.1016/0883-2927\(89\)90008-5](http://dx.doi.org/10.1016/0883-2927(89)90008-5)
- Prochaska, W., 1997. Die Bedeutung der chemischen Zusammensetzung von Einschlussfluiden und laugbaren Salzen für die Genese von hydrothermalen und sedimentären Karbonatgesteinen in den Ostalpen. *Mitteilungen der Österreichischen Geologischen Gesellschaft*, 90, 175-183.
- Prochaska, W., 2000. Magnesite and talc deposits in Austria. *Mineralia Slovaca*, 32, 543-548.
- Rantitsch, G., Grogger, W., Teichert, C., Ebner, F., Hofer, C., Maurer, E.M., Schafer, B. and Toth, M., 2004. Conversion of carbonaceous material to graphite within the Greywacke Zone of the Eastern Alps. *International Journal of Earth Science*, 93, 959-973. <http://dx.doi.org/10.1007/s00531-004-0436-1>
- Rantitsch, G., Sachsenhofer, R., Hasenhüttl, C., Russegger, B. and Rainer, T., 2005. Thermal evolution of an extensional detachment as constrained by organic metamorphic data and thermal modeling: Graz Palaeozoic Nappe Complex (Eastern Alps). *Tectonophysics*, 411, 57-72. <http://dx.doi.org/10.1016/j.tecto.2005.08.022>
- Ratschbacher, L., 1986. Kinematics of Austro-Alpine cover nappes: changing translation path due to transpression. *Tectonophysics*, 125, 335-356. [http://dx.doi.org/10.1016/0040-1951\(86\)90170-8](http://dx.doi.org/10.1016/0040-1951(86)90170-8)
- Ratschbacher, L., 1987. Stratigraphy, tectonics and paleogeography of the Veitsch nappe/Graywackezone, Eastern Alps, Austria: a rearrangement. *Mineralia Slovaca*, 5, 407-414.
- Ratschbacher, L., Merle, O., Davy, P. and Cobbold, P., 1991a. Lateral extrusion in the Eastern Alps: Part 1. Boundary conditions and experiments scaled for gravity. *Tectonics*, 10, 245-256. <http://dx.doi.org/10.1029/90TC02622>
- Ratschbacher, L., Frisch, W., Linzer, G. and Merle, O., 1991b. Lateral extrusion in the Eastern Alps: Part 2. Structural analysis. *Tectonics*, 10, 257-271. <http://dx.doi.org/10.1029/90TC02623>
- Ratschbacher, L. and Frisch, W., 1993. Palinspastic Reconstruction of the Pre-Triassic Basement Units in the Alps: The Eastern Alps. In: J. v. Raumer and F. Neubauer (eds.), *Pre-Mesozoic Geology in the Alps*. Springer, pp. 41- 51.
- Redlich, K., 1909. Die Typen der Magnesitlagerstätten. *Zeitschrift für praktische Geologie*, 17, 300-310.
- Reinecker, J., 2000. Stress and deformation: Miocene to present-day tectonics in the Eastern Alps. *Tübinger Geowissenschaftliche Arbeiten, Reihe A* 55, 128pp.
- Sachsenhofer, R.F.A., Lankreijer, A., Cloething, S. and Ebner, F., 1997. Subsidence analysis and quantitative basin modelling in the Styrian Basin (Pannonian Basin system, Austria). *Tectonophysics*, 272, 175-196. [http://dx.doi.org/10.1016/S0040-1951\(96\)00257-0](http://dx.doi.org/10.1016/S0040-1951(96)00257-0)
- Sachsenhofer, R.F.A., Dunkl, I., Hasenhüttl, C. and Jelen, B., 1998. Miocene thermal history of the southwestern margin of the Styrian Basin: Vitrinite reflectance and fission track data from the Pohorje/Kozjak area (Slovenia). *Tectonophysics*, 297, 17-29. [http://dx.doi.org/10.1016/0040-1951\(98\)00161-9](http://dx.doi.org/10.1016/0040-1951(98)00161-9)
- Sachsenhofer, R.F.A., Kogler, A., Polesny, H., Strauss, P. and Wagreich, M., 2000. The Neogene Fohnsdorf Basin: Basin formation and basin inversion during lateral extrusion in the Eastern Alps (Austria). *Geologische Rundschau*, 89, 415-430. <http://dx.doi.org/10.1007/s005310000083>
- Scharf, A., Handy, M.R., Favaro, S., Schmid, S.M. and Bertrand, A., 2013. Modes of orogen-parallel stretching and extensional exhumation in response to microplate indentation and roll-back subduction (Tauern Window, Eastern Alps), *International Journal of Earth Sciences (Geologische Rundschau)*. <http://dx.doi.org/10.1007/s00531-013-0894-4>
- Schmid, S., Fügenschuh, B., Kissling, E. and Schuster, R., 2004. Tectonic map and overall architecture of the Alpine orogen. *Eclogae Geologicae Helveticae*, 97, 93-117. <http://dx.doi.org/10.1007/s00015-004-1113-x>
- Schönlaub, H., 1981. Die Grauwackenzone in den Eisenerzer Alpen. *Jahrbuch der Geologischen Bundesanstalt*, 124, 361-423.
- Schroll, E., 1997. Geochemische und geochronologische Daten und Erläuterungen. In: Weber, L. (ed.), *Handbuch der Lagerstätten der Erze, Industriemineralien und Energierohstoffe Österreichs*. Geologische Bundesanstalt, 19, pp. 395-538.
- Schroll, E., 2002. Genesis of magnesite deposits in the view of isotope geochemistry. *Boletim Paranaense de Geociencias*, 50, 59-68.
- Schulz, B., Bombach, K., Pawlig, S. and Brätz, H., 2004. Neoproterozoic to Early-Paleozoic magmatic evolution in the Gondwana-derived Austroalpine basement to the south of the Tauern Window (Eastern Alps). *International Journal of Earth Science (Geologische Rundschau)*, 93, 824-843. <http://dx.doi.org/10.1007/s00531-004-0421-8>
- Schuster, R., and Frank, W., 1999. Metamorphic evolution of the Austroalpine units east of the Tauern Window: indications for Jurassic strike slip tectonics. *Mitteilungen der Gesellschaft der Geologie- und Bergbaustudenten in Österreich*, 42, 37-58.

- Schuster, R., Scharbert, S. and Abart, R., 1999. Permo-Triassic crustal extension during opening of the Neotethyan Ocean in the Austroalpine - Southalpine realm. *Tübinger Geowissenschaftliche Arbeiten - Serie A*, 52, 5-6.
- Schuster, R. and Stüwe, K., 2008. Permian metamorphic event in the Alps, *Geology* 36, 731 603-606. <http://dx.doi.org/10.1130/G24703A.1>
- Selverstone, J., 1988. Evidence for east-west crustal extension in the Eastern Alps: Implications for unroofing of the Tauern Window. *Tectonics*, 7, 87-105. <http://dx.doi.org/10.1029/TC007i001p00087>
- Spötl, C. and Vennemann, T. 2003. Continuous-ow isotope ratio mass spectrometric analysis of carbonate minerals. *Rapid Communications in Mass Spectrometry*, 17, 1004-1006.
- Thöni, M., 2006. Dating eclogite-facies metamorphism in the Eastern Alps – 769 approaches, results, interpretations: a review. *Mineralogy and Petrology*, 88, 123–148. <http://dx.doi.org/10.1007/s00710-006-0153-5>
- Tollmann, A., 1977. *Geologie von Österreich - Die Zentralalpen* (Deuticke).
- Valley, J., Bohlen, S., Essene, E. and Lamb, W., 1990. Metamorphism in the Adirondacks. *Journal of Petrology*, 31, 555-596. <http://dx.doi.org/10.1093/petrology/31.3.555>
- Wagreich, M., 1995. Subduction tectonic erosion and Late Cretaceous subsidence along the northern Austroalpine margin (eastern Alps, Austria). *Tectonophysics*, 242, 63-78. [http://dx.doi.org/10.1016/0040-1951\(94\)00151-X](http://dx.doi.org/10.1016/0040-1951(94)00151-X)
- Wang, X. and Neubauer, F., 1996. Orogen - parallel strike - slip faults bordering metamorphic core complexes: The Salzach-Enns fault zone in the Eastern Alps, Austria. *Journal of Structural Geology*, 20, 799-818. [http://dx.doi.org/10.1016/S0191-8141\(98\)00013-3](http://dx.doi.org/10.1016/S0191-8141(98)00013-3)
- Willingshofer, E., Neubauer, F. and Cloetingh, S., 1999a. The Significance of Gosau-Type Basins for the Late Cretaceous Tectonic History of the Alpine- Carpathian Belt. *Physics and Chemistry of the Earth*, 24, 687-695. [http://dx.doi.org/10.1016/S1464-1895\(99\)00100-3](http://dx.doi.org/10.1016/S1464-1895(99)00100-3)
- Willingshofer, E., van Wees, J. and Cloetingh, S., 1999b. Thermomechanical consequences of Cretaceous continent-continent collision in the eastern Alps (Austria): Insights from two dimensional modeling. *Tectonics*, 18, 809-826. <http://dx.doi.org/10.1029/1999TC900017>
- Wölfler, A., Kurz, W., Danišić, M. and Rabitsch, R., 2010. Dating of fault zone activity by 803 apatite fission track and apatite (U-Th)/He thermochronometry: a case study from the Lavanttal fault system (Eastern Alps). *Terra Nova*, 22, 274–282.
- Wölfler, A., Kurz, W., Fritz, H. and Stüwe, K., 2011. Lateral extrusion in the Eastern Alps revisited: refining the model by thermochronological, sedimentary and seismic data, *Tectonics*, 30 TC4006. <http://dx.doi.org/10.1029/2010TC002782>
- Wölfler, A., Stüwe, K., Danišić, M. and Evans, N.J., 2012. Low temperature thermochronology in the Eastern Alps: Implications for structural and topographic evolution, *Tectonophysics*. <http://dx.doi.org/10.1016/j.tecto.2012.03.016>

Received: 28 March 2014

Accepted: 29 September 2014

Anke WÖFLER^{1*)}, Walter PROCHASKA¹⁾ & Harald FRITZ²⁾

¹⁾ University of Leoben, Peter-Tunner-Str. 5, 8700 Leoben, Austria;

²⁾ University of Graz, Heinrichstr. 26, 8010 Graz, Austria;

^{*)} Corresponding author, anke.woelfler@unileoben.ac.at